The use of compliant materials in thrust bearings

P. Bradford

THE USE OF COMPLIANT MATERIALS IN THRUST BEARINGS

by

P. BRADFORD

Thesis submitted for the degree of M.Sc. to the University of Durham

Department of Mechanical Engineering

Sunderland Polytechnic

September 1975

SUMMARY

This project is concerned with the possibility of utilising the elastic properties of a plastic material to form the converging surface, required for the successful operation of a thrust pad.

A method was devised to form an inclined pad surface, without involving accurate machining processes, the profile of which is modified under the action of the hydrodynamic pressure generated in the lubricant.

A model investigation was undertaken, the results being presented in the form of dimensionless groups. These results show that, over part of the operating range, the compliant pad has a better load carrying capacity than that of the inclined plane slider.

A simple mathematical model was postulated, the results of which compare fairly well with those obtained from the experimental programme.

ACKNOWLEDGEMENTS

I wish to record my gratitude to all those persons who have been connected in any way with this research project and the production of the thesis, especially the technical staff of the Department of Mechanical Engineering of Sunderland Polytechnic.

Especial thanks are due to my supervisor, Professor G.R. Higginson, for the guidance and constructive comments which hd contributed during the course of the research.

ACKNOWLEDGEMENTS

I wish to record my gratitude to all those persons who have been connected in any way with this research project and the production of the thesis, especially the technical staff of the Department of Mechanical Engineering of Sunderland Polytechnic.

Especial thanks are due to my supervisor, Professor G.R. Higginson, for the guidance and constructive comments which hd contributed during the course of the research.

CONTENTS

Notation

Δ	original distortion of the pad leading edge	m
δ	distortion under hydrody namic pressure	m
Y	deflection of the outlet edge of the pad	m
h	film thickness	m
L	pad length	m
B	pad breadth	m
C	pad depth	m
K	convergence factor	
μ	viscosity	$N\text{-}S/m^2$
u	runner velocity	m/S
$\bar{P}$	mean pad pressure	N/m^2
Cl	leakage coeficient	
E	modulus of elasticity in compression	N/m^2
λ	deflection coeficient	
h_o	outlet film thickness	m
C	depth of pad	m
ϵ =	initial strain of the pad leading edge	

Dimensionless groups

Ho	$= \frac{ho}{\Delta}$	
P	$= \bar{p}c/E\Delta$	pressure number
U	$= \mu u/E\Delta$	velocity number
V	$= 1.25U/\epsilon^2$	modified velocity number

Plate 1.

View of the compliant pad in operation.

CHAPTER 1

1.1 Introduction

The hydrodynamic theory of lubrication, as presented by Osborne Reynolds (1) following the experimental investigations of Beauchamp Tower (2), has shown that effective lubrication of two load-carrying surfaces, with relative motion, requires a wedge-shaped space between the surfaces, whereupon a pressure is generated in the lubricant which forms a film separating the surfaces. Generally the lack of any such convergence in the parallel-surface thrust bearings then in use accounted for their poor load-carrying capacity. Nevertheless it has been shown (3) that a parallel-surface thrust bearing can carry a considerable load, under certain conditions, the necessary convergence being caused by thermal distortion due to temperature gradients in the bearing pad.

The tilting pad thrust bearing, introduced by Michell (4) in 1905, not only formed the convergence in a simple way, but also automatically adjusted the degree of convergence to an optimum value, depending on changes in the applied load or sliding velocity.

Another method of forming the required convergence of the bearing surfaces, often used in large water turbine bearings, is to machine a slope on the thrust pad leaving a small proportion of the pad length parallel to the runner in order to reduce the wear of the pad under conditions of starting and stopping. In this type of bearing the degree of convergence of the pad is constant so that under "off-design" operating

conditions the bearing is not running with an optimum film thickness.

Both the fixed and tilting pad bearings can, theoretically, only operate successfully for a fixed direction of the relative motion between the bearing surfaces, although, by moving the pivot point to a central location, the tilting pad can operate in either direction with little loss of load carrying capacity compared with the conventional pivot location (5). This apparent anomaly has been explained by considering the thermal and elastic distortions of the pad to form a convergent oil film without the bearing necessarily tilting (5),(6).

These experimental and theoretical studies have led several researchers to investigate particular designs of thrust pad in which a section is cut away from the non-working face, the converging wedge being formed by elastic distortion. A.H. Bennet and C. Ettles (1) have described the operation of a 'cantilever' bearing, figure 1, which has a performance similar to the conventional pivoted pad.

An experimental investigation was reported by E.W. Hemingway (8) in which a portion of the underside of the pad was removed leaving rigid support for the trailing edge and the sides of a deflecting diaphram, figure 2. This produces a variation in film thickness in the radial direction which reduces the side flow of the lubricant resulting in a load carrying capacity of this type of bearing somewhat superior to that of the pivoted pad.

These experimental and theoretical studies of the performance characteristics of thrust bearing pads demonstrate

that the generation of the pressure in the lubricant is sensitive to the physical shape and dimensions of the wedge which can be affected by both thermal and elastic distortions. This requires that the items which make up a thrust bearing containing a number of pads must be manufactured to fine tolerances, and then carefully assembled.

The manufacturing process also includes a 'tinning' process by which the pad working surfaces are coated with a white metal. Thus the manufacturing costs of thrust bearings can be large compared with plain bearings.

The present trends in pad configuration are aimed at reducing the complexities, and the cost, by eliminating the pivot by using the elastic distortion of the pad to form the wedge. The configurations reviewed still require machining to fairly close limits and still incorporate a white metal surface coating.

It is the purpose of this investigation to examine the possibility of using the load-bearing and elastic properties of a modern plastic material in order to eliminate the need for the provision of the pivot and the white metal coating but still retain good load carrying characteristics.

The intention is to form the pads in a thick disc of the plastic material by cutting radial slots at suitable angular intervals. The inlet side of each pad could then be permanently contracted by some form of clamping arrangement thus forming a wedge-shaped lubricant space with the runner, shown in figure 3. The pressure generated in the lubricant film will then modify the profile of the working surface of the pad with the possibility

of the film thickness ratio remaining approximately constant over a limited range of load.

There is a further possibility of the pad distorting in the transverse direction. This should have the effect of shrouding the sides of the pad thus reducing the side leakage to some extent.

CHAPTER 2

Design and Manufacture of the test equipment

2.1 Full scale testing

When investigating the performance of thrust pads under conditions of hydrodynamic lubrication problems can arise which mask the basic principles involved. The root cause of these difficulties is the frictional heating of both the oil, as it passes through the bearing, and the surfaces in contact with the oil, thus distorting the surface profile. The viscosity of the lubricant, which is sensitive to temperature, can vary considerably between the inlet and outlet edges of the pad and so the effective value to be used in the presentation of the results, usually by dimensionless groups, is open to conjecture.

The measurement of small clearances which exist between the sliding surfaces require sophisticated and expensive equipment, mainly electronic gauging, which depend for their operation on the electrical or magnetic properties of the bearing material and as this investigation is concerned with the feasibility of using non-conducting and non-magnetic plastic material to form the bearing surface then the difficulty is enhanced.

The cost of manufacturing a full scale test-rig and the associated equipment, and the work load that it would have imposed on the workshop, was prohibitive at the time when this investigation was started. Thus a programme of model tests of limited objectives was decided upon, using, as far as possible, apparatus already existing in the department.

2.2 Model Tests

The use of a model pad is intended to reduce the variation in the lubricant viscosity through the pad and the consequent thermal distortion by reducing the frictional heating, to increase the film thickness and reduce the pressure in the lubricant film so that they can be measured by simple instruments.

2.3 Pad Form

Figure (6) shows a schematic diagram of the form of the pad finally adopted. The deformable pad (B) was made from a rubber which could be cast, and cured at a low temperature, onto a supporting plate (A) which transferred the applied load from a lever arrangement (figure 5) through the pivots (K) to the pad. The pivots, being on the longtitudinal axis of the pad, allowed the pad to level itself in the transverse direction under the action of the hydrodynamic pressure generated in the lubricant film acting on the surface of the pad.

In order to create a convergent film, a bar was cast into the rubber at the inlet edge (F), two rods were screwed into the bar so that they passed vertically through the pad and supporting plate. Tapped holes were provided in the supporting plate so that the rods could be locked by the set screws (E). The pad was then loaded so that the depth of the pad between the supporting plate and the pad surface contracted, the rods were then locked in this position and the load removed. The depth of the pad at the leading edge remained at the initial value but increased towards the outlet edge of the pad, thus forming

a converging wedge with the moving surface.

In order to measure subsequent deflections of the pad under working conditions, small diameter pins were cast into the pad but were attached only to the pad at the lower extremities, the upper ends projected through holes drilled into the supporting plate. A datum line was attached to the supporting plate so that relative movement between the pins and the datum line could be measured by a travelling microscope, figure 4. This relative movement was the deflection of the working surface of the pad. It was found necessary to fix small beads of araldite, coated with primer, to the lower ends of the pins to prevent the pins working loose. Each pin was made from 'hypodermic' steel tubing of 1.5mm diameter, one end of which was ground to form a chamfer. This provided a curved surface in the image in the telescope, facililating the positioning of the cross-hair of the microscope eyepiece.

2.4 Order of Magnitude analysis

For the purpose of this analysis the assumption is made that the load-carrying capacity of the compliant pad is similar to that of the tilting pad, neglecting side leakage. Thus the relationship between the mean pad pressure and the optimum film thickness at the outlet edge is given by

$$\frac{\bar{P}\, h_o^2}{\mu u L} = 0.158 \qquad \text{ref. 9}$$

In practice h_o is the order of 0.02mm, now if the value of h_o is restricted to 0.5mm for the model tests, an increase of twenty-five fold, then the average pressure is reduced by a

factor of 625 and can thus be measured by simple mercury manometry. If the bearing speed, lubricant viscosity and dimensions of the pad are specified, then the temperature variation of the lubricant is given by the relationship

$$t = \frac{\mu u L}{\rho c h_o^2} \times 1.15 = \frac{\bar{p}}{\rho c} \times 7.25$$

and so the temperature rise will also be reduced by a factor of 625 and is considered negligible.

Various lubricants were used, the most viscous being castor oil with a viscosity of 1 N-S/m^2 at a temperature of 21°C. The rig was a modified machine manufactured by S. Dennison & Co., with a maximum belt speed of 1 m/s, and could accommodate a pad of length 100mm, thus for a minimum oil film thickness of 0.5mm the average pressure on the pad is of the order of 6KN/m^2.

2.5 Pad deflection

In order to determine the magnitude of the deflections of the pad to be expected, again assume that the pad operates as a tilting pad without side leakage. Consider the pad operating under a mean pressure of 1.6 KN/m^2 then the outlet film thickness would be 1mm with an inlet film thickness of 2mm. Now consider the mean pressure on the pad to be increased to 6.3 KN/m^2. If the film thickness ratio is to remain at a value of 2 then the inlet film thickness would be 1mm and the outlet film thickness 0.5mm. Thus, as the inlet edge does not deflect then the outlet edge must deform by an amount equal to 0.5mm. If it is further assumed that the deflection at the outlet edge is the same as would occur under a uniform pressure equal to the mean pad

pressure then the estimate of the required modulus of compression can be made as the pad is required to deflect 0.5mm under an increase in pressure of (6.3 - 1.6) KN/m^2. The depth of the pad was fixed at 80mm, therefore the required modulus of compression is $4.7 \times 10^3 \times 80 \times 10^{-3} / 0.5 \times 10^{-3}$ i.e. about 750 KN/m^2. A suitable material was chosen, a silicone rubber manufactured by I.C.I., which had a modulus of 980 kN/m^2.

2.6 Test Rig

A simplified general arrangement of the machine is shown in figure (5).

This apparatus was adapted from a rig manufactured by the firm of S. Dennison & Co., for teaching purposes. The modifications were such that they did not interfere with that function. The moving surface of the model was provided by an endless nylon belt (A) which ran over two rollers B & C one of which (B) was driven, via a hydraulic variable speed device (D), by a one-half horsepower electric motor (E) connected to the 220v 50Hz. mains supply. The combination of the variable drive unit and the belt and pulley system enabled the speed of the belt to be varied between zero and 1 m/s. The part of the belt passing beneath the thrust pad, being subjected to the hydrodynamic lubricant pressure, was supported by a plate (F) attached to the frame of the machine. The nylon belt dipped into a reservoir of oil and carried a thick film of the lubricant to the pad. It was found that the oil supply to the pad was more than sufficient to give full lubrication. Each

roller was fitted to a shaft which rotated in ball bearings mounted in brackets attached to the frame. The bearing brackets of the idling roller were so attached to the frame that the centre distance between the rollers could be altered in order to adjust the tension in the nylon belt so that it did not slip on the driving roller. The driving roller was also grooved axially to prevent an oil film being generated between it and the belt.

The model thrust pad (G) was suspended over the nylon belt by means of a cradle pivoted to two brackets (H) which were bolted to the frame of the machine. The cradle was formed by two levers (I) bolted together by a spacing bar (J), which allowed only relative angular movement between the levers, and the pad was attached to the cradle by pivots (K) located on its longtitudinal axis and passing through the levers. The weights of the cradle and pad assembly were counterbalanced by a weak spring (L) hooked to the spacing. The pad was loaded by standard laboratory weights added to the pan (M) which hung from the spacing bar. This arrangement allowed the pad to move vertically, due to the hydrodynamic pressure generated in the oil film, and also tilt in the direction of the motion of the belt depending on the position of the weight pan on the spacing bar. The oil reservoir, formed from narrow gauge sheet steel, fitted round the rollers and nylon belt. One side of the reservoir was slotted to allow the shaft carrying the driving roller to pass through, the oil level being below the slot.

It was found that, during an extended test run, the temperature of the oil slowly increased continuously, temperature

rises of 20°C being common, due to the shearing of the oil by the nylon belt. This caused thermal distortion of the pad and thus certain parameters, required to be constant for a series of tests, altered. This difficulty was eliminated by fitting a cooling-water tube in the base of the reservoir. The temperature of the oil could then be maintained at a constant value to within 5°C above ambient.

The deflections of the pad, oil film thickness, and the 'setting up' of the pad were measured by a travelling microscope (N) which was situated on a platform (O) attached to the side of the machine. The microscope slideway was placed parallel to the longtitudinal axis of the pad and could be tilted in any desired direction by means of the three adjusting screws (P) in the base. The vertical movement of the microscope was measured by-means of a dial gauge graduated in divisions of 10^{-2}mm. A mercury thermometer (Q) was placed in the oil at the inlet edge of the pad and to one side where the depth of the oil, due to the damming action of the pad, was sufficient to cover the thermometer bulb.

2.7 Manufacture of the model pad

In section 2.5 the order of magnitude analysis indicated the required Modulus of Compression to satisfy pad deflection and film thickness requirements. The material used was Silcoloid 201, a liquid silicone rubber compound which cured at room temperature when mixed with the appropriate curing agent. The curing process could be accelerated by increasing the temperature of the rubber, 60°C being the recommended value.

This material would only adhere to other components if they were first coated with a primer before casting the pad. A useful property of the rubber was its transparency, enabling the conditions of lubrication within the oil gap to be viewed through the side of the pad. If the pad was starved of lubrication then total internal reflection of the light occurred at any point where an incomplete film existed, this region appeared as a silvery patch.

A square pad of dimensions 100mm x 100mm with a thickness of 80mm was chosen, this being the maximum size which the rig could accommodate. A diagram of the pad assembly is shown in figure (6). The rubber pad (B) was cast onto a perspex supporting plate (A) which was coated with primer. The supporting plate was provided with a series of holes of 6mm diameter (C), a further two holes of 2mm diameter (D) along the longtitudinal axis of the plate and two holes of (E) 6mm diameter. A perspex bar of 12mm square section, with one face machined at an angle to provide a straight and definite edge, was cemented onto the upper face of the supporting plate in order to provide a datum line used in the measurements of the pad deflections. A mould (figure 7) was made from four sheets of perspex cemented together, the supporting plate was attached to the mould to form the fifth side, the remaining side was left open to the atmosphere. Steel rods of suitable size were inserted through the holes (C) to act as cores. A perspex bar (F), provided with two tapped holes (G) was lightly fixed to the inside face of the mould and coated with primer. Two steel rods (H) with threaded ends were passed through the holes E and screwed into the tapped

holes G. All the holes and gaps were sealed with a plastic compound and the faces of the mould and the steel rods were coated with a release agent.

The mixture of rubber and the curing agent was deaerated in a vacuum chamber for fifteen minutes and then poured slowly into the mould to avoid entraining any air. The rubber was then part-cured at room temperature for 48 hours to allow the rubber to set and then given a final curing time of five hours in an oven at a temperature of 60°C. The plastic compound sealing the possible leakage paths softened at this temperature but the rubber was already cured enough not to leak.

The mould and the cores were then removed and the pad was suspended over a flat glass plate A shown in figure (8). One edge of the supporting plate rested on a set of slip gauges (B) and the other rested on the arm of a vernier depth gauge (C), the clearance between the bottom of the pad and the glass plate being about 2mm. The pins for measuring the movement of the pad surface were then positioned in the holes in the pad left by the removal of the cores.

In order to ensure that the datum edge on the pad supporting plate was parallel with the plane of the glass plate, the following procedure was adopted. A probe (D) was inserted in the appropriate hole (F) in the pad supporting plate, its lower extremity resting on the glass plate. The travelling microscope, with its slideway placed parallel to the longtitudinal axis of the pad, was adjusted vertically until the crosshair in the microscope eyepiece just touched the magnified image of the upper end of the probe. The probe was then removed and replaced

in the appropriate hole in the trailing edge of the supporting plate, and the microscope was then moved along the slideway until the image of the probe was again seen in the eyepiece, the adjusting screws on the base of the microscope were used to move the microscope until the crosshair again touched the probe image. This procedure was repeated with the probe alternately positioned in the holes in the leading and trailing edges of the pad until further adjustment of the microscope base screws was unnecessary, the microscope then moved parallel to the glass plate.

The microscope was then focussed on the datum line on the pad supporting plate and the vernier depth gauge was adjusted until the crosshair of the microscope remained on the image of the datum line when the microscope was moved along the slideway. The pad supporting plate was then parallel to the glass plate.

A rectangular collar (E), made from perspex sheet, was placed on the glass plate circumscribing the pad, thus forming a mould round the pad. Rubber was then poured into this mould to a depth of four millimetres and allowed to cure.

The pad was then removed from the glass plate and the surplus rubber, round the edge of the pad, was cut off with a sharp knife.

The pad was then ready to be placed in the test rig.

CHAPTER 3

Measurement and Procedure

3.1 Pad adjustment

The pad supporting plate was kept parallel to the surface of the belt under all the varying conditions of load and belt speed, in order to simulate the conditions under which a single pad would operate in a full-scale thrust bearing. In order to achieve this object, the microscope slideway was made parallel to the belt using the procedure outlined in section 2.6. When this was done with the belt in motion then the microscope slide was only parallel to a line joining the two points where the probes touched the belt as the belt deflected slightly between these two points due to the oil pressure in the film. The pad supporting plate could then be made parallel to the microscope slide by focussing the microscope on the datum line on the plate and adjusting the position of the weight pad on the spacing bar so tilting the pad until the microscope could be moved along the slide without the crosshair leaving the image of the datum line. The complete procedure only occupied a time of about five minutes.

It was sometimes required that the pad was to be levelled under zero load conditions and the belt stationary. In this case the spacing bar was loaded in a vertical direction until the arms of the cradle contacted adjustable stops, not shown in diagram (5). The pad was tilted by altering the adjustment of those stops.

3.2 Measurement of film thickness

In order to measure the film thickness along the pad, probes were made from stainless steel 'piano' wire of diameter slightly less than the internal diameter of the hypodermic tubing used for the pad-deflection pins. The probes were given a slight initial curvature so that, when inserted in the hypodermic tubes, they tended to stick a little and were not forced out by the pressure in the lubricant.

A glass plate was placed on the nylon belt and positioned under the pad. A mass of 1kg was placed in the weight pan which pressed the pad surface against the glass plate. The pad was then levelled and the distance between the ends of the probes and their respective tubes was measured by the vertical movement of the microscope. This gave a datum value for zero clearance between the pad surface and the belt at each probe position. Under test conditions, with the belt moving, the probes were gently pushed down the tubes until they just touched the belt, a slight vibration of the pin could be sensed manually at this point. The difference in heights of the probe and the tube were again measured by the microscope. The difference between these values and their respective datum values for zero clearance gave the clearance between the pad surface and the belt under working conditions. This measurement was repeatable to $\pm$ 3 x 10^{-2}mm with the belt in motion whereas with the belt stationary it was repeatable to within $\pm$ 1 x 10^{-2}mm. The increase in error was attributed to the vibration of the rig with the motor running.

As the film thickness measurement depended on the difference in two separate readings then the errors will accumulate

according to the square root of the sum of the squares of the individual errors, assuming a normal distribution. Thus the error expected for the value of the film thickness is given by

$$e = 10^{-2}\sqrt{3^2 + 1^2} = 3.16 \times 10^{-2}\text{mm} = \underline{3.5 \times 10^{-2}\text{mm}}$$

this could represent an error of nearly 10% for some film thickness encountered under heavy loads or low velocities, but in general represented less than 4%.

3.3 Measurement of Load

The pad was loaded by weight pan and standard laboratory weights acting through the lever arrangement, as shown in figure (5) with a mechanical advantage of 14:3. The pad and cradle assembly were balanced by the spring (L) which was lowered until the trailing edge of the pad just touched the belt.

At low loads and a high belt velocity the cradle could lift by as much as 1mm and as the spring length could only be measured to the nearest millimetre then the inaccuracy in the value of the applied load could be as high as 0.125N in 5N i.e. $2\frac{1}{2}$%, but in most cases was less than 1%.

Another cause of error would be friction in the pivots holding the cradle to the frame of the machine. Assuming a coeficient of friction as high as 0.3 although the pin is boundary lubricated, then the error is 1%.

3.4 Measurement of belt speed

The speed of the nylon belt was measured by timing a given number of revolutions of the belt by a hand operated stop-watch. The number of revolutions was determined by counting the number

of times a mark on the belt passed a stationary datum on the frame of the rig.

This method of speed measurement had two apparent disadvantages. The value of the belt speed was not an instantenous value and the process of setting the speed to a predetermined value, one of trail and error, a tedious and lengthy procedure. These disadvantages were obviated for the following reasons. The methods adopted for measuring the other variables gave only average values, e.g. film thickness, due to the inertia of the system so that only the average value of the velocity was required.

The experimental procedure adopted required the load on the pad to be constant and the speed varied, thus the value of the speed did not need to be accuratly predetermined.

In order to calculate the belt speed, the length of the belt was measured. A strip of melinex was attached to the belt by the surface tension of a thin smear of oil and the point at which the ends overlapped was marked and the distance subsequently measured. If L is the length of the belt in metres and N is the number of revolutions in a time interval of T seconds then the belt velocity is given by

$$U = \frac{NL}{T}$$

To estimate the error in the value of U calculated, likely errors in the values of N, L, and T are assumed.

The stop watch was graduated in 0.2 second intervals therefore assuming a reading error of $\pm$ 0.1S in a total of fifteen seconds, the minimum time interval then

$$\delta U = -\frac{NL}{T^2}\,\delta T = -\frac{U}{T}\,\delta T$$

$$\therefore \delta U/U = \delta T/T$$

thus the error would be .1/15 x 100% ≃ .67%. A further error to be considered is the reaction time of the operator in manipulating the stopwatch at both the start and finish of the timing sequence, but it is considered that these errors cancel each other.

The error in the measurement of the length of the belt is assumed to be ± 2mm then

$$U = N/T\ \delta L = U/L\ \delta L$$

$$\therefore \delta U/U = \delta L/L$$

$$= 2/1082 \times 100 \simeq 0.2\%$$

Therefore the expected error in the calculated belt speed

$$= \sqrt{.2^2 + .61^2} = \underline{0.7\%}$$

3.5 Measurement of pressure

The probes were removed from the hypodermic tubing and perspex tubes were inserted into the holes in the pad supporting plate, to a depth of 6mm, to form pressure tappings. Flexible acrylic tubing connected the pressure tappings to a multitube mercury manameter which could be read to ± 1/2mm. The air was bled from the tubes before the readings were taken.

It was found that the mercury levels were taking a long time to reach a steady reading, due to the hypodermic tubing offering a large resistance to the flow of the oil required to displace the mercury. It was decided, therefore, to extract

the hypodermic tubing by cutting out that part of the pad constraining the tubing with a small diameter cork boring tool. This modification considerably shortened the time taken for the mercury levels to reach equilibrium. The hypodermic tubes had to be recast into the pad after each series of pressure tests.

3.6 Measurement of the Modulus of Compression

A block of the pad material was cast to the same dimensions as the model thrust pad and positioned between two smooth and greased metal plates. The upper plate was progressively loaded, the loads being hung on hangers which were equally spaced from the centreline of the block. The deflection of the block was measured by a dial gauge and noted for each increment of load. The slope of the resulting stress against strain characteristic gave the modulus of elasticity of the block in compression. The value of 980 kN/m^2 was repeatable to within $\pm$ 1%.

The block was left under load for three hours at a constant temperature, but no creep was observed over this time interval.

3.7 Measurement of Lubricant Viscosity

The viscosity of the oil over a range of temperatures was measured in a standard U-tube viscometer, calibrated by the manufacturer, placed in a constant temperature water bath. The result was repeatable to within 0.5%.

3.8 Design of Experiment

The outlet film thickness, h_o, depends on the geometry of the pad (L, B, c, Δ), the lubricant viscosity, μ, the speed of

the belt, V, the elasticity of the pad, E, and the load on the pad defined by the average pressure $\bar{P}$

i.e. h_o = function of $(L, B, c, \Delta, \mu, V, E, \bar{P})$

using Δ , V and E as the repeating variables in an analysis of the dimensions then:-

$$h_o/\Delta = f([L/\Delta],[B/\Delta],[c/\Delta],[\mu V/E\Delta],[\bar{P}/E])$$

This expression can be re-arranged by multiplying several of the π - terms together thus

$$h_o/\Delta = f([B/L],[c/L],[\Delta/c],[\mu U/E\Delta],[\bar{P}c/E\Delta])$$

In this series of model tests L, b, and C are kept constant.

Hence $$\frac{h_o}{\Delta} = f([\Delta/c],[\mu U/E\Delta],[\bar{P}c/E\Delta])$$

the term Δ/c is the initial strain ϵ of the leading side of the pad.

The group $\frac{E\Delta}{c}$ is the uniform pressure $\hat{P}$ required to deflect the pad by an amount Δ therefore the non dimensional group $\bar{P}c/E\Delta$ can be written $\bar{P}/\hat{P}$ and has an upper limit on its value of unity. The term $\mu U/E\Delta$ relates the velocity and lubricant properties to the elastic properties of the pad, denote this term as U, denote h_o/Δ as H_o

thus $$H_o = f(\epsilon, U, P)$$

ϵ can be varied by varying Δ and can be held constant but cannot easily be set to a predetermined value. U can be varied and can be held constant but not easily to a predetermined value.

In order to compare the performance of the different geometrical forms of the pad it would be better to re-arrange

the equation further, by extracting Δ from the first and third terms

$$\text{i.e.} \quad h_o/L = f\left((\Delta/C), \left(\frac{\mu u}{\bar{p}C}\right), \left(\frac{\bar{p}C}{E\Delta}\right) \right)$$

Now the term $\mu u/\bar{p}C$ can be further modified by noting $\bar{p} = \frac{W}{b\bar{L}}$ and replacing C by b thus giving $\frac{\mu u L}{W}$ the reciprocal of which is frequently used in presenting bearing characteristics and is termed the 'duty parameter'. Hence an alternative arrangement of the variables gives

$$h_o/L = f\left((\Delta/C), \left(\frac{W}{\mu u L}\right), (\bar{p}/\hat{p}) \right)$$

3.9 Experimental procedure

As shown in the previous section, the variation in the outlet film thickness with the independent variables could be presented in the form

$$h_o/L = \text{function of} \left((\Delta/C), \left(\frac{W}{\mu L u}\right), (\bar{p}/\hat{p}) \right)$$

It was therefore decided to divide the test programme into groups each with a constant but differing value of Δ/C. Each group was further divided into sets, each with a constant but differing value of $\bar{p}/\hat{p}$. Thus each set consisted of the variation in h_o/L with the duty parameter $\frac{W}{\mu L u}$. The duty parameter was varied by varying u, the belt speed.

The test programme was ordered in the following stages:-

i. The initial deformation was developed.

ii. The pad was loaded and then levelled with the nylon belt in motion. The belt motion was never initiated with the pad in contact with the belt as there was a high coeficient of friction between the pad and the belt and the ensuing high shear stress caused damage to the pad surface.

iii. The rig was left running for sometime in order that the bulk temperature of the oil could reach a steady value.

iv. Readings of the pad datum, probe, and hypodermic tube levels were taken, by use of the microscope, then the oil temperature and the belt velocity were measured.

v. The belt velocity was altered and stage iv was repeated. The datum line on the pad supporting plate was levelled, if required, before readings were taken. This procedure was repeated for several values of the belt velocity.

vi. The load on the pad was increased and stages iv and v were repeated. This procedure was repeated for several values of load.

vii. The initial deformation of the pad was altered and the above process repeated.

Formation of the initial pad height was carried out with the nylon belt stationary, but with the pad located in the cradle. The weight pan was loaded to a predetermined value and the pad was levelled as described in section 3.1. The set screws in the pad supporting plate were then tightened, locking the inlet edge of the pad in this loaded position, the load was then removed, leaving the working surface of the pad in a distorted form.

In order to determine this distorted form and the value of the pad height Δ , a glass plate was placed beneath the pad and resting on the nylon belt. The arms of the cradle were forced against the adjustable stops and the pad levelled with the glass plate. The clearance between the surfaces was then measured. The pad height could then be calculated by taking the difference between the values of the clearance at the inlet and outlet edges. The pad height could not be set accurately to a predetermined value but a rough guide for the load required to produce a given height could be estimated from

$$\text{Load} \simeq E \times \Delta \times \text{pad area/depth of the pad C.}$$

CHAPTER 4

4.1 Analysis of the Elastic Pad

It is well known that the load carrying capacity of various film shapes is affected largely by the ratio of the inlet to outlet film thickness and to a lesser degree by the actual shape of the film.

Let the deflection of the outlet edge under the action of the lubricant pressure be

$$Y = \frac{\lambda \bar{P} C}{E}$$

The relationship between h_1 h_o Δ and Y can be expressed by

$$\delta = \Delta - Y \qquad \text{but} \qquad \delta = h_1 - h_o$$

hence $h_1 - h_o = \Delta - Y$

or $K = \frac{1}{h_o} \{ \Delta - Y \}$

therefore $K = \frac{1}{h_o} \{ \Delta - \lambda \bar{P} C/E \}$

which can be re-arranged to give

$$K = \frac{\Delta}{h_o} \times \left\{ 1 - \frac{\bar{P}c}{E\Delta} \right\}$$

Now the term $\frac{E\Delta}{C}$ is the uniform pressure required to deform the pad by an amount Δ, this being an upper limit to the allowable mean pressure on the pad. As the film thickness is evaluated along the centre line of the pad then $\bar{P}$ in the above equation refers to the mean value of the centreline pressure, if the effects of side leakage are to be considered then this is different from the value of load on the pad/area and so is replaced by

$\bar{P}/C_1$ where $\bar{P}$ is the overall mean pressure and C_1 is the side leakage coeficient.

$$\text{thus } K = \frac{\Delta}{h_o} \times \left[1 - \frac{\lambda \bar{P}}{C_1 \hat{P}} \right] \quad \text{where } \hat{P} = E\Delta/C$$

On using the same notation as in section 3.8

$$K = \frac{1}{H_o}\left[1 - \frac{\lambda}{C_1} P \right] \qquad \text{with } \bar{P}/\hat{P} = P \quad (3.0)$$

Assuming that the load carrying capacity is the same as that for the inclined pad for which

$$\frac{Ph_o^2}{UL} = C_1 \text{ func (K)}$$

func. (K) is well documented (ref 9.)

Now writing $\bar{P} = \frac{E\Delta}{C}$, $h_o = H_o\Delta$, $uU = E\Delta U$, $L = 1.25C$

and $C = \Delta/$

then $$\frac{PH_o^2}{1.25\ U/^2} = C_1 \text{ func (K)}$$

or if $1.25\ U/^2$ is written as V then

$$\frac{PH_o^2}{V} = C_1 \text{ func. (K)} \qquad (3.1)$$

Equations 3.0 and 3.1 can be evaluated to give the relationship between P, H_o, and V, but, before this can be accomplished, estimates of λ and C_1 are required.

4.2 Compression of rectangular blocks by a non-uniform pressure distribution

The analysis of the load-carrying capacity of the previous section requires the relationship between the deflection at the outlet edge of the pad and the mean pressure applied to the pad.

The solutions of two-dimensional problems in elasticity are frequently sought by means of the Airy Stress function satisfying the biharmonic equation

$$\frac{\partial^4\phi}{\partial x^4} + 2\frac{\partial^4\phi}{\partial x^2\partial y^2} + \frac{\partial^4\phi}{\partial y^4} = 0$$

Where the stress components are given by

$$\sigma_x = \frac{\partial^2\phi}{\partial y^2}, \quad \sigma_y = \frac{\partial^2\phi}{\partial x^2}, \quad \tau_{xy} = -\frac{\partial^2\phi}{\partial x\,\partial y}$$

This can be shown(10) to be the equivalent to determining a form of ϕ which makes the strain-energy of the block a minimum.

The strain energy of the block is given by

$$V = \frac{1}{2E}\iint\{\sigma_x^2 + \sigma_y^2 - 2\nu\sigma_x\sigma_y + 2(1+\nu)\tau_{xy}^2\}\,dx.dy.$$

as the stress distribution does not depend on the elastic constants of the material the ν can be set at zero therefore

$$V = \iint\{\sigma_x^2 + \sigma_y^2 + 2\tau_{xy}^2\}$$

or $$V = \iint\left(\left(\frac{\partial^2\phi}{\partial y^2}\right)^2 + \left(\frac{\partial^2\phi}{\partial x^2}\right)^2 + \left(\frac{\partial^2\phi}{\partial x\partial y}\right)^2\right)dx.dy.$$

The problem is to find ϕ as a function of x and y which will make (4.4) a minimum and satisfy the loading on the boundaries. In order to simplify the problem it was assumed that the pad was subject to the same stress distribution as a block of twice the

depth of the pad and loaded symmetrically about the y axis as shown in figure (9).

It was further assumed that the resulting distortion could be superimposed on the original distortion and that one did not affect the other. The final assumption made was that the pressure distribution on the boundary could be expressed as a polynomial in y and remained of this form despite variation in the convergence factor K.

J.N. Goodier[10] outlined an approximate method for the stress analysis of a loaded block which can be modified to solve the present model.

The form of the solution sought is of the form

$$\phi = \sum_{0}^{n} a_n \phi_n \qquad (4.5)$$ in which $a_0 = 1$ and

ϕ_0 satisfies only the boundary conditions, whereas ϕ_1, ϕ_2, etc., give no contribution to the stresses at the boundaries and contain the adjustable constants a_n by which the strain energy is made a minimum. Substituting (4.5) into (4.4) gives a function containing a_n^2 and the condition that V is to be a minimum, that is

$$\frac{\partial V}{\partial a_n} = 0 \qquad (4.6)$$

gives a set of linear equations in a_n. The stresses derived from (4.5) are

$$\sigma_x = \frac{\partial^2 \phi}{\partial y^2} = \frac{\partial^2 \phi_0}{\partial y^2} + \sum a_n \frac{\partial^2 \phi_n}{\partial y^2}$$

$$\sigma_y = \frac{\partial^2 \phi}{\partial x^2} = \frac{\partial^2 \phi_0}{\partial x^2} + \sum a_n \frac{\partial^2 \phi_n}{\partial x^2} \qquad (4.7)$$

$$\tau_{xy} = -\frac{\partial^2 \phi}{\partial x \partial y} = -\frac{\partial^2 \phi_o}{\partial x \partial y} - \sum a_n \frac{\partial^2 \phi}{\partial x \partial y}$$

In the present problem the sides $y = \pm b$ are free from applied stresses and sides $x = \pm a$ are assumed free from shear stresses, the effect of the viscous shear stress being considered negligible compared with the effect of the pressure. Thus $\frac{\partial^2 \phi_o}{\partial x^2} = -\frac{\partial^2 \phi_o}{\partial x \partial y} = 0$

and $\frac{\partial^2 \phi_o}{\partial y^2}$ is the assumed hydrodynamic pressure distribution applied to the sides $X = \pm a$. Substituting equations 4.7 into 4.4 and differentiating the integrand for the condition of minimum strain energy then, on re-arranging

$$\iint \left[\frac{\partial^2 \phi_n}{\partial y^2} \sum a_n \frac{\partial^2 \phi_n}{\partial y^2} + \frac{\partial^2 \phi_n}{\partial x^2} \sum a_n \frac{\partial^2 \phi_n}{\partial x^2} + 2 \frac{\partial^2 \phi_n}{\partial x \partial y} \sum a_n \frac{\partial^2 \phi_n}{\partial x \partial y} \right] dx.dy =$$

$$= \iint \frac{\partial^2 \phi_o}{\partial y^2} \cdot \frac{\partial^2 \phi_n}{\partial y^2} dx.dy$$

Which gives a set of linear equations for the a_n

For the rectangle bounded by $x = \pm a$ and $y \pm b$ the form of the stress function is most conveniently taken as

$$\phi = \phi_o + (x^2-a^2)^2 (y^2-b^2)^2 \left[a_1 + a_2 x^2 + a_3 y^2 \right]$$

for a symmetrical stress distribution about $X = 0$.

Limiting the analysis to the first term containing a_1 only then $\phi = \phi_o + (x^2-a^2)^2 (y^2-b^2)^2 a_1$ (4.9)

and for an asymmetrical distribution about $x = o$

$$\phi = \phi_o + (x^2-a^2)^2 (y^2-b^2)^2 a_1 y \qquad (4.10)$$

For the symmetrical case

$$\sigma_x = \frac{\partial^2 \phi_0}{\partial y^2} + 4\, a_1 (x^2-a^2)^2 (3y^2-b^2)$$

$$\sigma_y = 4\, a_1 (y^2-b^2)^2 (3x^2-a^2) \qquad (4.11)$$

$$\tau_{xy} = -16\, a_1 xy (y^2-b^2)(x^2-a^2)$$

Thus $\sigma_{y=o}$ on the side $y = b$ $\tau_{xy} = o$ on all sides and the stress on the surface $x = a$ is simply $\frac{\partial^2 \phi_0}{\partial y^2}$, on substituting (4.11) into (4.8) one linear equation in a_1 results

$$\left[\frac{64}{7} + \frac{256}{49}\frac{b^2}{a} + \frac{64}{7}\frac{b^4}{a^4}\right] a_1 = -\frac{9.5.5}{128\, a^9 b^5} \iint \frac{\partial^2 \phi_0}{\partial y^2} 4(x^2-a^2)(3y^2-b^2) \qquad (4.12)$$

The pressure distribution applied to the sides $x \pm a$ is assumed to be of the form

$$P = S\left[\left(1 - \frac{y^2}{b^2}\right) + \frac{1}{2}\left(\frac{y}{b}\right)\left(1 - \frac{y^2}{b^2}\right)\right] \qquad (4.13)$$

A graph of this pressure curve is shown in figure (4.1) which is shown to be slightly displaced from a parabolic distribution.

thus $\sigma_{xo} = S + \frac{S}{2}\frac{y}{b} - S\frac{y^2}{b^2} - \frac{S}{2}\frac{y^3}{b^3} = \frac{\partial^2 \phi_0}{\partial y^2}$

Considering the stresses produced by the symmetrical term Sy^2/b^2, substituting into (4.12)

$$a_1\left\{\frac{64}{7}+\frac{256}{49}\left[\frac{b}{a}\right]^2+\frac{64}{7}\left[\frac{b}{a}\right]^4\right\} = -\frac{9.5.5}{128}\frac{1}{a^9b^5}\int_0^a\int_0^b 4S\frac{y^2}{b^2}(x^2-a^2)(3y^2-b^2)\,dx.dy$$

$$= -\frac{1}{a^4b^2}$$

Now $\frac{b}{a} = \frac{5}{8}$

hence $\underline{a_1 = -0.0796}$ $\frac{1}{a^4b^2}$

The stresses produced by the symmetrical term S are uniform (ie $a = 0$)

Considering asymmetrical terms, the stress function (4.10) is used, resulting in an expression analagous to (4.8)

$$\left\{\frac{64}{7}+\frac{256}{105}\left[\frac{b}{a}\right]^2+\frac{64}{55}\left[\frac{b}{a}\right]^4\right\}a_1b = -\frac{975}{128}\frac{1}{a^9b^5}\int_0^a\int_0^b \frac{\partial^2\phi_0}{\partial y^2}.\frac{\partial\phi_1}{\partial y^2}.dx.dy \qquad (4.14)$$

and the stress components

$$\sigma_x = \frac{\partial^2\phi_0}{\partial y^2} + 4a_1\left[x^2-a^2\right]\left[5y^3-3b^2y\right]$$

$$\sigma_y = 4\,a_1(y^2-b^2)^2y\,(3x^2-a^2) \qquad (4.15)$$

$$\tau_{xy} = 2a_1\left(x^2-a^2\right)(x)\left(5y^4-6b^4y^2+b^4\right)$$

For the term $\frac{S}{2}\frac{Y}{b}$ the stresses are linear ($a_1 = 0$)

thus the final term to be considered is $\frac{S}{2}\frac{y^3}{b^3}$

which on substitution into (4.14) gives, for a_1

$$-\frac{S}{2} \times 0.0585$$

Thus $\sigma_x = \left(\frac{S}{2}\frac{y^3}{b^3} - \frac{S}{2}\cdot\frac{0.0585}{a^4b^3}\cdot 4.(x^2-a^2)^2(5y^2-3by^2)\right)$

On adding the components of the stresses together for each of the terms of the polynomial approximation to the pressure distribution

$$\sigma_x = S\left[1-\frac{y^2}{b^2}+\frac{y}{2b}\left(1-\frac{y^2}{b^2}\right)+\left\{0.278\left(3\frac{y^2}{b^2}-1\right)+0.117\left(5\frac{y^3}{b^3}-3\frac{y}{b}\right)\right\}\left(\frac{x^2}{a^2}-1\right)\right] \qquad (4.16)$$

To obtain the deflection U in the x direction

$$E\frac{dU}{dx} = \sigma_x - v\sigma_y$$

$$\therefore \; EU = \int_0^a \sigma_x dx - \int_0^a v\sigma_y dx$$

it can be seen that $\int_0^a \sigma_y dx = 0$ at $x = 0$ and a

and can be neglected.

Thus (4.16) integrated and the limits inserted gives for the deflection of the side x = a relative to the $\mathbb{C}$ of the block, writing y/b = Y

$$U = \frac{Sa}{E}\left[(1-Y^2)+\frac{1}{2}Y(1-Y^2)+\left\{.148\,(3Y^2-1)+.0625\,(5Y^3-3Y)\right\}\right]$$

Thus the deflection at the trailing edge of the pad is given by the value of U at Y = 1

$$U_o = \frac{Sa}{E} \quad 0.421$$

The mean value of the pressure curve $\bar{P} = \frac{2}{3}S$

therefore the deflection of the outlet edge of the pad, in terms of the mean pressure, is, therefore

$$U_o = 0.63\,\frac{\bar{P}A}{E}$$

or $\lambda = 0.63$

The pressure distribution

$$= S \left\{ (1-Y^2) + \frac{Y}{2} (1-Y^2) \right\} \qquad Y = 2\frac{X}{L} - 1$$

has been used to evaluate the deflection of the outlet edge of the pad, but the pressure distribution alters with the inlet/outlet film thickness ratio. To approximate to this variation let

$$= S (1-Y^2) + BY (1-Y^2)$$

Where B assumes a value such that the centre of pressure of the assumed distribution coincides with that for the pressure distribution for an inclined pad.

On integrating the above expression and inserting the limits of

$$Y = \pm 1 \qquad \bar{P} = \frac{2}{3} S$$

then as $\bar{P}\,\bar{Y} = \frac{1}{2} \int_{-1}^{+1} P\, Y dY$

$$\therefore \bar{Y} = \frac{3}{4} \frac{S}{S} \int_{-1}^{+1} \left[Y - Y^3 + BY^2 - BY^3 \right] dY$$

$$= \frac{B}{5}$$

hence $\underline{B = 5\bar{Y}} \qquad \left(\bar{Y} = 2\bar{X} - 1\right)$

where $\bar{x}$ is taken from published results.

Table 3.0 gives the values for B for values of K.

κ	$\bar{x}$	B	λ
0.5	.6	.4	.6
1	.66	.7	.7
1.5	.715	.9	.77
2	.75	1.07	.81
3	.8	1.4	.95
4	.835	1.54	1.05

Table 3.0

4.3 Side Flow

4.31 Reynolds equation

Reynolds equation for the variation in the hydrodynamic pressure generated between two surfaces, with relative motion, separated by a lubricant can be shown to be:-

$$\frac{\partial}{\partial x}\left[h^3\frac{\partial p}{\partial x}\right] + \frac{\partial}{\partial y}\left[h^3\frac{\partial p}{\partial y}\right] = \frac{\partial h}{\partial x}[6\mu u]$$

This equation cannot normally be integrated directly to obtain the pressure as a function of x and y. It is possible to obtain an approximate solution only by making a drastic simplification of the mathematics. In this instance the assumption is made that the term $h^3\frac{\partial p}{\partial y}$ is constant in the y-direction. This is equivalent to assuming that the flow in the y-direction, the side flow, is constant over one half of the pad. This assumption overlooks the fact that the flow in the y-direction should be zero at y equal to zero but the constant flow can be thought of as an approximate average of the overall side flow.

Thus the second term in Reynolds equation is zero and the remaining terms, if solved along the centre-line of the bearing, give the same solution for the pressure as that for an infinitely wide bearing.

Now h varies across the pad depending on the pressure function, making two more assumptions necessary in order to be able to integrate the above expression. The assumptions made are:-

a) that the variation in film thickness across the pad can be approximated by the function

$$h = h_c\left[1 - \frac{m}{B/2}y\right] \text{ in the region } 0<y<B/2 \qquad (4.15)$$

Where h_c is the film thickness on the pad centre line and 'm' is a constant to be determined later.

b) that the difference between the film thickness on the centre line and the film thickness at the edge of the pad is due to a parabolic pressure distribution and can be calculated by the method of section 4.2.

Thus the expression for the deflection is

$$U = \frac{Sc}{E} \left(1-Y^2 + .148 \left\{ 3Y^2-1 \right\} \right)$$

In the present case $Y = y/2B$ and $S = P_c$ the pressure on the centreline.

Deflection on the centreline $U_c = \frac{P_c C}{E} \left(1 - .148 \left(-2 \right) \right)_{Y=0}$

$$= .704 \frac{P_c C}{E}$$

Deflection at the edge of the pad $U_e = \frac{P_c C}{E} \left(.296 \right)$

and so the difference in the film thickness at the centreline and the edge of the pad is given by

$$U_c - U_e = 0.408 \frac{P_c C}{E} \qquad (4.16)$$

Now the assumed film shape, expression 4.15, gives, for the difference in film thickness at $y = o$ and $y = \frac{B}{2}$

$$h_c - h_e = h_c - h_c (1 - m) = m h_c$$

and so $m h_c = 0.408 P_c C/E$

and so $$m = \frac{0.408 P_c C}{h_c E} \qquad (4.17)$$

The pressure variation across the pad can now be estimated

$$h^3 \frac{dp}{dy} = \text{Constant } (q)$$

and on substituting $h = h_c \left(1 - \frac{m}{B/2} y\right)$

then

$$P = \frac{q}{h^3 c} \left(\int \frac{dy}{\left[1 - \frac{my}{B/2}\right]^3} \right) + \text{Const.}$$

which, on integration and insertion of the boundary conditions

$P = 0$ at $y = B/2$ and $P = P_c$ at $y = 0$

gives $$P = \frac{P_c}{m(2-m)} \left(1 - \frac{(1-m)^2}{\left[1 - \frac{my}{B/2}\right]^2} \right) \qquad (4.18)$$

In order to find the load carried by the pad, the average pressure across the pad is required

the mean pressure across the pad $= \frac{2}{B} \int_0^{B/2} P dy$

$$= 2/B \; \frac{P_c}{m(2-m)} \; 1 - \frac{(1-m)^2}{\left[1 - \frac{my}{B/2}\right]^2} \; dy$$

$$= \frac{P_c}{(2-m)} \qquad (4.19)$$

Thus expression 4.19 gives the mean pressure across any transverse section along the pad in terms of a leakage coeficient ($^{1}/_{2-m}$) multiplied by the pressure at the centre line of the pad, which has been assumed to be the same as the pressure given by an infinitely wide flat inclined pad. This leakage factor can vary along the pad depending upon the value of P_c/h_c at any section, but if an average value is used then a

$$P_{av} = {}_{A}\int P_c \, dA$$

$$\text{i.e. } P_{av} = \frac{1}{2-m}\frac{1}{L}\int_0^L p_c \, dx$$

$$\text{or } \bar{P}_{av} = \frac{1}{2-m}\left(P_{av}\right)_{\text{theoretical}}$$

thus $\frac{1}{2-m}$ becomes the overall leakage coeficient C_1

Evaluating m at the point at which the maximum pressure occurs

$$\text{i.e. from expression 4.17 } \quad m = 0.41\frac{C}{E}\frac{P_c}{h_c}$$

but for a flat inclined pad

$$P_{max} = \frac{6\mu UL}{h_o^2}\left[\frac{K}{4(K+1)(K+2)}\right]$$

and $\bar{h}_c = 2\frac{(K+1)}{(K+2)}h_o$

thus the required ratio of $\frac{P_c}{h_c}$ is

$$\frac{P_c}{\bar{h}_c} = \frac{6\mu UL}{ho^3}\left[\frac{K}{8(K+1)^2}\right]$$

Now as $W^* = \frac{\bar{P}\,h_o^2}{\mu UL}$ substituting in the above

expression gives

$$\frac{\hat{P}_c}{\bar{h}_c} = \left[\frac{2}{3}\left(\frac{K}{(K+1)^2}\right)\frac{1}{W^*}\right]\frac{\bar{P}}{h_o}$$

Now if values of K are substituted, with the appropriate value of W^* then it is seen that term in the brackets does not vary much

K	1	2	3	4	5
$P_c/\bar{h}_c$	1.05	1	1.01	1.02	1.06

thus, using a value of 1.06, then

$$\frac{P_c}{h_c} \simeq 1.06 \quad \frac{\bar{P}}{h_o}$$

On substituting in expression 4.17

$$= .43 \quad (\bar{P}/h_o)(C/E)$$

and so $C_1 = 1/(2 - .43\ \bar{P}/H_o)$ 4.20

4.4 Load Carrying Capacity

On returning to expression 4.0

$$K = \frac{1}{H_0}\left(1 - \frac{\lambda}{C_1} P\right) \qquad 4.0$$

it has been found that λ varies with K (section 4.2), the numerical results given in table (30) on page 34

A simple straight line law, i.e.

$\lambda = 0.6 + 0.1K$ shown on graph (4.2)

adequately describes that variation.

Thus the expression for K, equation 4.0, can be modified to give

$$K = \frac{P}{H_0}\left[\frac{\frac{1}{P} - \frac{0.6}{C_1}}{1-0.1\left[\frac{P}{H_0}\frac{1}{C_1}\right]}\right] \qquad (4.21)$$

Expression 4.1 can be re-arranged to give

$$V = \frac{P\ H_0^2}{\text{func}\,(K)\ C_1} \qquad (4.22)$$

Then the three equations 4,20, 4.21 and 4.22 can be solved numerically to provide the relationship between H_0 P and V. The numerical solution of these three expressions is readily accomplished by dividing the calculation into the following steps:-

a) Choose a range of P, and for each value of P,

b) Choose a range of H_o, and for each value of H_o,

c) Calculate the ratio P/H_o, then using these values of P, H_o, P/H_o calculate

i) C_1 from expression 4.20

ii) K from expression 4.21

iii) read the value of W* from the graph at that value of K obtained in (Cii)

iv) calculate V from expression 4.22

The results of this computation are shown in graph (4.0)

In order to facilitate the presentation and the comparison of these results, an empirical relationship of the form $H_o = A\, V^n\, P^m$, is fitted to the above results. For each value of the load number P, the variation of H_o with the velocity number V is expressed as

$$H_o = \bar{B}\, V^n$$

There are two unknown quantities in the expression requiring two points on the graph to be used in their determination, the empirical curve will obviously pass through these two points, but will also pass through the origin, so in fact there are three accuracy points. The two points on the graph were chosen according to the 'Chebyshev Spacing' rule appendix (A6.4) in an attempt to minimise the errors. Thus a value for n was found for each curve of constant pressure, these values did not differ greatly, so an average value for all the curves was taken and found to be 0.42. Hence each characteristic has the form $H_o = \bar{B}V^{0.42}$ where $\bar{B}$ varies with the pressure, graph (4.3) shows this variation. Using accuracy points of P = 0.25 and 0.55, the variation is closely approximated by the empirical expression

$$\bar{B} = 0.368\ P^{-0.388}$$

The complete family of characteristics can now be expressed by

$$H_o = 0.358 \; V^{.42}/P^{.388} \qquad (4.23)$$

In order to compare the theoretical with the experimental results the above expression is plotted on a graph (5.19) in the form

$$P^{.388} \; H_o = \text{function } V$$

$$(= .358V^{.42} \text{ for the theoretical case})$$

to give but a single characteristic.

CHAPTER 5

EXPERIMENTAL RESULTS AND DISCUSSION

5.1 Variation in outlet film thickness with runner velocity

The variations in outlet film thickness with changes in the runner velocity are displayed, on graphs 5.0, 5.1 and 5.2, as constant applied load characteristics for each of the three values of initial pad height. The viscosity of the lubricant was under partial control by means of varying the cooling water flow rate, but the accurate maintenance of a constant value of viscosity from test to test was not possible so the graphs are plotted to a base of viscosity x velocity. The largest pad height was 3.63mm which corresponded to a strain of 4.5% which is about the maximum strain to which plastic materials can be subjected without the phenomena of creep becoming a problem and was much higher than that envisaged for a full-scale pad.

It was found that the bearing pad could only be loaded up to a certain value whereafter a further increase in load caused the pad to 'fail'. This maximum value of load depended on the pad height and increased with increase in the pad height. The applied load at the point of this pad instability represented a value of the non-dimensional pressure number, P, of 0.6. The mode of failure seemed to be the sudden expansion of the outlet portion of the pad causing it to tilt and contact the belt. Variation in the runner velocity made no difference to the load causing failure.

The reasons for this phenomenon were the subject of a later

investigation.

5.2 Variation in outlet film thickness with applied load

Graphs 5.3, 5.4 and 5.5 are derived from the previous results and show the variation of the outlet film thickness with the applied load, in the form of the mean applied pressure, for three values of constant runner velocity. Each of the characteristics exhibits, initially, a form typical of those of other types of thrust pads, but at the higher pressures, corresponding to a value of P of 0.4, there is a point of inflection in each of the curves. In order to check the shape of these characteristics, a further series of tests were performed in which the velocity of the runner was maintained at a constant value while the applied load was increased. The results are displayed on graph 5.11 and the characteristic again shows a point of inflection at a value of P in the region of 0.4 after which the curve droops and instability of the pad again occured at a value of P in the region of 0.6.

5.3 Comparison between the load carrying capacity of the compliant pad and the theoretical characteristics of the inclined plane slider

The variation in outlet film thickness with applied pressure, for a constant value of runner velocity, is displayed on one graph (graph 5.6) for the three pad heights. Graphs 5.7 and 5.8 are similar characteristics for differing constant values of runner velocity.

The characteristics for the inclined plane slider are also displayed on these graphs. Curve A is the theoretical

variation in outlet film thickness with increasing applied pressure for an inclined plane slider, of infinite width, at its optimum slope. Curve B is the theoretical characteristic with side leakage taken into consideration.

It can be seen that, within the limits of experimental error, the individual film thickness characteristics follow closely the same curve up to that point of inflection noted previously.

The set of characteristics, for the highest value of runner velocity, displayed on graph 5.6 run fairly closely to curve B for the lower values of applied pressure but tend to give higher values of outlet film thickness, at the higher pressures, than those predicted for the plane tilting pad with side leakage. The improved values of outlet film thickness characteristics is more marked at the lower values of runner velocity as shown on graphs 5.7 and 5.8. Indeed at the low velocity the set of characteristics runs quite close to the theoretical curve for the tilting pad of infinite width. This improved performance occurs only to those pressures corresponding to a value of 0.4 for the dimensionless pressure number P, whereafter the improvement diminishes.

5.4 Variation in film thickness parameter with the duty parameter

Graphs 5.9, 5.10 and 5.11 display the results in the form of the dimensionless groups derived in section 3.8. The term W/ UL is often used in presenting bearing performance characteristics and is known as the 'duty parameter'. Again the performance characteristics for the tilting pad, with and without side leakage, are shown. For each of the pad

heights tested, the variation in outlet film thickness is plotted against the duty parameter for constant values of the pressure number. It is evident that no single curve is produced, as for the tilting pad, and that the film thickness is dependent not only on the duty parameter, but also on the pressure number.

5.5 Pad profile and pressure curves

In this series of experiments all the deflection probe readings were noted in order to ascertain the geometry of the bearing surface under differing load conditions but with the runner velocity maintained at a constant value. The results of this series of tests are displayed on graph 5.12 in which the height of the pad is shown using an imaginary line, drawn through the inlet edge and running parallel to the runner velocity, as a datum. The profile of the pad under conditions of zero load were measured with the runner stationary. At low pressures the pad surface is convex, gradually flattening until a value of P between 0.2 and 0.3 is reached whereupon parts of the pad, towards the trailing edge, become concave. At a value of P of 0.5 this concavity is most pronounced.

The deflection probes were then removed, the pressure tappings inserted and the series of tests repeated at the same runner velocity and for the same values of load used in the previous tests. The results for the film shape and the pressure profiles for the increments of load are shown on graph 5.13. Also shown are the equivalent plane slider profiles which would occur for the same values of inlet and outlet film

thickness. The value of K varies little over the range of load, remaining at a value of just under unity. The pressure profiles tend to be more symmetrical than those for the tilting pad, especially at the lower loads, but the point of maximum pressure moves slightly towards the trailing edge as the load increases. The concave portion of the pad is seen to occur in the region of maximum pressure.

Further pad profiles were obtained with differing pad heights and are depicted on graphs 5.14 and 5.15 all of the profiles show the same tendency to concavity at the higher loads, although this effect diminishes with increasing pad height.

5.6 Pad instability

The problem of the apparent failure of the pad to carry loads over a certain value was the subject of two further sequences of tests, in which the pad height and the runner velocity were held constant. In the first sequence of tests, the load was applied to the pad, via the cradle, by the loading hanger. The lubricant pressure at stations along the centreline of the pad was noted for each increment of load upto the load causing failure. In the second sequence of tests the pad was loaded by means of the adjustable stops, the pressure profile again being recorded for each value of outlet film thickness thus obtained. No instability of the pad was observed during this series of tests, the stops could be adjusted to such an extent that the lubricant was wiped from the belt.

The mean pressure along the centreline of the pad was

calculated for each pressure profile using the trapezaidal rule. The variation in outlet film thickness was plotted against the mean pressure for both sequences of tests on graph 5.18. The characteristic for both series of tests coincide up to the load which caused the pad to fail in the first sequence, a value corresponding to a pressure number of 0.56 but this is based on the mean pressure along the centre-line, not the overall pad pressure. The characteristic for the second sequence of tests continues, in an almost linear form, down to zero outlet film thickness at a pressure number of 0.9.

5.7 Discussion of the experimental results

On inspection of graphs 5.6, 5.7 and 5.8, which compare the outlet film thickness against mean pad pressure characteristics for the compliant pad with the theoretical predictions for a plain slider bearing tilted to its optimum slope, it is evident that the compliant pad performs as well as the tilting pad with side leakage at the higher runner velocities or lower pad pressures. As the runner velocity is reduced, or the pressure is increased, the characteristics for the compliant pad approach that of the ideal tilting pad, and, although the shape of the pad profile will alter slightly as the inlet to outlet film ratio increases with reducing velocity, it is thought that the improvement is due to reduced side leakage at the lower outlet film thicknesses. This reduction in side leakage is effected by the pad being of a concave shape in a direction transverse to the direction of

motion of the runner, due to the pressure distribution in the lubricant across the pad, which, in effect, shrouds the bearing.

At any particular value of the mean applied pressure the film thickness along the pad centreline reduces as the velocity of the runner is reduced, but as the difference in film thickness between the centreline and the side of the pad remains approximately constant, then the shrouding effect is increased.

It is evident that the changing pad geometry under the effects of load makes the usual single curve of minimum film thickness with duty parameter in-appropriate, as shown by the distinct separation between the constant applied load curves of graphs 5.9, 5.10 and 5.11 for the three different pad heights. These curves again show that the compliant pad gives a greater value of minimum oil film thickness than the tilting pad over the range of operation limited by the pressure number of about 0.6.

The outlet film thickness with mean pressure characteristics for the three pad heights and for all values of constant velocity exhibit a point of inflection in the curve corresponding to a pressure number of 0.4, inspection of the graphs 5.12 to 5.14 displaying the pad profile shows a marked concavity of the pad surface at this pressure number. Now graph 5.13 gives the results of a series of tests for a constant runner velocity in which the inlet to outlet film thickness ratio remained appreciably constant over the range of load. The value of the load carrying capacity W^* is also displayed and is plotted

against a pressure number on graph 5.17. It is evident that the load carrying capacity increases up to a pressure number of 0.4 and decreases sharply thereafter, even though the value of K is reasonably constant. This is in contradiction of the assumption, frequently made, that, once the inlet to outlet film ratio is fixed, then the load carrying capacity of the pad is reasonably independent of the shape of the lubricant film. This disagreement is thought to be caused by the concave nature of the pad surface. It is, therefore, inferred that, as the pressure on the pad is increased then a point is reached where the resulting deformation of the pad gives a profile which is unfavourable to the generation of pressure within the lubricant film. The load carrying capacity number sharply decreases after this point causing the inflection in the curves of film thickness at outlet - V - applied pressure.

Graph 5.16 shows the variation in outlet film thickness with variation in the mean pressure along the pad centreline, with the load being applied in the same way as all of the previous tests in which pad failure was experienced and with the load being applied in a different manner, through the use of the adjustable stops. These characteristics exhibit the same change of slope as noted in previous tests but whereas the tests in which the pad was loaded by the hanger again encountered pad failure, the series utilising the adjustable stops encountered no such instability, therefore the cause of the pad failure must lie in the manner of loading the pad. It has been observed that the pad failed when the pressure

number reached a value in the region of 0.6, the pad profile near this value is shown in graph 5.14 and it can be seen that the pad surface has a region of pronounced concavity. It is thought, therefore, that any small variations of the pad from the horizontal plane, due to the adjustment of the pad as outlined in section 3.1 or to vibrations in the rig, cause the centre of pressure to move towards the trailing edge which gives rise to an unbalanced turning moment on the pad about a transverse axis. The leading edge of the pad is then forced towards the runner which further adversley affects the pressure profile resulting in the failure of the pad to carry the load.

5.8 Comparison between Experimental and Theoretical Models

The comparison between the prediction from the theoretical analysis and the results of the experimental investigation is made on graph 5.19 by plotting the values given by both of the models in the grouping $P^{\cdot 388}H_o$ as a function of V as the theory predicts that

$$P^{\cdot 388}H_o = 0.358V^{\cdot 42}$$

The estimated error band is also plotted, based on the computation of the above expression A6.1 , and it evidently encompasses most of the experimental points. The rather wide error band is caused by the error in the value of Δ , used in the calculation of the groups, which is thought to be due to the variations in bulk temperature of the pad causing the trailing edge of the pad to expand. The room temperature could vary by $5^{\circ}F$ during a series of tests and, due to the poor

location of the rig the sun's radiation would cause further temperature changes.

The range of the experimental results used in the comparison is limited to those for which the value of P is less than 0.4 because, as shown in section 5.7, for values greater than this the load carrying capacity of the pad sharply diminishes for constant film ratio hence the assumption used in the derivation of expression 3.0, that the load capacity is independent of the shape of the pad for a given film ratio, is no longer valid. This diminution of load capacity of a pad of concave profile can be shown by assuming the profile to be given by the relationship

$$h/h_o = 2/2 - (x/L)^n \quad \text{for a film ratio of 2}$$

and by varying n between 0 and say 4 then the profile changes from concave to convex and the load capacity reaches a peak. A6.2

The value of the pressure number P can also be estimated from the theoretical model by assuming that the load capacity diminishes when the deflection of the pad, at its mid-length, is of such a value that the film thickness at this point is equal to that for the equivalent flat pad, and that the initial distortion of the pad at this point is zero. The value of P thus predicted A6.3 is 0.35 which amply supports the conclusions reached from the experimental evidence. [Section 5.6]

5.9 Further Work

As this model investigation obviated the problems associated with the frictional heating of the lubricant, then a full scale investigation is required to determine the effects of the temperature on compliant materials which could be used in a practical form of the pad.

One such material is 'Delrin', which has a modulus in compression of 5×10^4 lb /in^2. In common with most plastics, 'Delrin' has a high coeficient of expansion, the modulus decreases with increasing temperature, and creep effects. Delrin is available in differing forms which have differing coeficients of expansion and it may, therefore, be possible to isolate the effects of thermal expansion on the bearing performance.

Further investigation into the possibility of using this type of pad in Journal bearings as an alternative to the tilting pad type as it may improve the pressure profile by delaying the onset of cavitation, and could delay the onset of the whirling phenomena by suitable design.

5.10 CONCLUSION

The results of the experimental investigation of the characteristics of a compliant thrust pad show that this type of pad can have a superior load carrying capacity to a conventional plane inclined pad over part of its operating range limited to values of pressure number of 0.4.

The load carrying capacity, minimum film thickness and

sliding velocity can be related by the expression

$$P^{.388} H_o = 0.358 V^{.42}$$

which has been derived from a mathematical model for which the experimental model gave some justification to the simplifying assumptions used.

6.0 APPENDICES

6.1 Estimation of error band

Assuming accurate values of h_o P and U the error which has the largest effect on the computed values of P, H_o and V is that for Δ .

The ambient temperature could vary by $\pm 3^{\circ}C$ assume that the sun's radiation could vary the bulk pad temperature by a further $\pm 3^{\circ}C$ ∴ Total variation could be $\pm 6^{\circ}C$.

Coeficient of linear expansion of pad material

$$= 3.5 \times 10^{-4} \quad mm/mm^{\circ}c$$

∴ total variation $= \pm 3.5 \times 10^{-4} \times 80 \times 6$

$$= 2 \times 840 \times 10^{-4} mm$$

$$= .168mm$$

for $\Delta = 1.4mm$ $\quad \frac{\delta\Delta}{\Delta} \simeq 12\%$

$\Delta = 363mm$ $\quad \frac{\delta\Delta}{\Delta} \simeq 5\%$

for $\psi = P^{.388} H_o$ $\qquad \psi$ = the func.V

effect of δP on ψ $\qquad \frac{\delta\psi}{\psi} = .\frac{388}{P} \delta P$

P varies between .1 and .4

but $dP/P = \delta\Delta/\Delta \simeq 12\% \rightarrow 5\%$

$$\left(\frac{\delta\psi}{\psi}\right)_p \simeq 4.8\% \rightarrow 2\%$$

effect of δH_o on ψ $\quad \frac{\delta\psi}{\psi} = \frac{\delta H_o}{H_o} = \frac{\delta\Delta}{\Delta} = 12\% \rightarrow 5\%$

$\therefore$ likely effect $\frac{\delta\psi}{\psi}$ adding the above effects

$\therefore$ with $\Delta = 1.40\text{mm}$ $\frac{\delta\psi}{\psi} = \pm 17\%$

$\Delta = 3.63\text{mm}$ $\frac{\delta\psi}{\psi} = \pm 7\ \%$

effect on V $\quad V = \frac{\lambda u \ c^2}{1.25\ E\ \Delta^3}$ $\quad \therefore \frac{dV}{} = 3V \frac{\delta\Delta}{\Delta}$

$\therefore \frac{dV}{V} = 3 \frac{\delta\Delta}{\Delta}$

$\therefore$ at $\Delta = 1.40\text{mm}$ $\frac{dV}{V} = \pm 36\%$

$\Delta = 363\text{mm}$ $\frac{dV}{V} = \pm 15\%$

These errors are applied to V = 2 region in which $\Delta = 1.4\text{mm}$

and V = .1 region in which $\Delta = 3.63\text{mm}$

6.2 Effect of Surface Profile

In order to simplify the calculations take the film ratio at 2.

Profiles generated by $h/h_o = 2/(2 - \left[\frac{x}{L}\right]^n)$

or $\quad h^x = 2/(2-x^n)$ $\quad h^x = h/h_o$

$x = x/l$

now $\frac{dP^x}{dX} = \frac{\bar{h}^x}{h^{x3}} - \frac{1}{h^{x2}}$ Reynolds integrated equation

$$\therefore \quad \frac{dp^x}{dX} = \frac{\bar{h}^x}{8}\left[(2-X^n)^3 - 2(2-X^n)^2\right] \qquad p^x = \frac{ph_o^2}{6UuL}$$

with the boundary conditions P = 0 at X = 0 and 1

the above expression integrates to

$$p^x = \frac{1}{8}\left[8\beta X - \frac{4(1+3\beta)}{n+1}X^{n+1} + \frac{2(2+3\beta)}{2n+1}X^{2n+1} - \frac{(1+\beta)}{3n+1}X^{3n+1}\right]$$

and

$$\bar{h}^x = \frac{8 - 8/n+1 + 2/2n+1}{8 - 12/n+1 + 6/2n+1 - 1/3n+1} \qquad \beta = \bar{h}^x - 1$$

on integrating W^x

$$W^x = \int_0^1 p^x\,dX \qquad W^x = \frac{\bar{p}h_o^2}{UuL}$$

$$W^x = \left[4\beta - \frac{4(1+3\beta)}{(n+1)(n+2)} + \frac{2(2+3\beta)}{(2n+1)(2n+2)} - \frac{(1+\beta)}{(3n+1)(3n+2)}\right]\frac{2}{3}$$

6.3

The results of the computation are given in table 6.4

n	β	W*
.333	.524	.106
.7	.324	.15
1	.244	.156
1.5	.173	.164
2	.134	.16

TABLE 6.1

A6.3 Estimation of the critical pressure No.

Referring to figure 10, assume that the point at which the load capacity is a maximum when point A on the undeformed profile is deflected by the pressure to A^1.

Assume point A is at the same pad height as the trailing edge B in the undeformed state.

$$h_o = h_1 - \Delta + y_o \qquad \text{by geometry}$$

$$h_c = h_1 - \Delta + y_c$$

$$h_c = \frac{h_1 + h_o}{2}$$

on eliminating h_1 and h_o

$$2y_c - y_o = \Delta$$

Now the pad deflection at a point $= \lambda \frac{P_c}{E}$

Where λ is a deflection coeficient and P is the pressure on the centreline at that point.

thus $$\frac{P_c}{E} \left[2\lambda_c - \lambda_o \right] = \Delta$$

or $\div \Delta$ and recognising P_c/E = P on the ℄

$$P = \frac{1}{2\lambda_c - \lambda_o}$$

In section 4.2 the pad deflections for an assumed pressure distribution are determined, from which $\lambda_c = 2\lambda_o$

$$\therefore \quad P = 1/3\lambda_c$$

but λ_o is a function of the film ratio. Taking a value for λ_o for a film ratio of 2 i.e. $\lambda_o = 0.7$

then $P = 1/2.1 = 0.48$

but this value is that for the mean pressure at the centreline of the pad, to obtain an overall mean pressure, the above value should be multiplied by the leakage coeficient. Taking representative values of V and P of 2 and 0.4 respectively, a value of $C_1 \simeq 0.7$ is obtained and hence

$$P = 0.34$$

which is remarkably close to the experimental findings in view of the simplifying assumptions made.

6.4 The Chebyshev spacing rule

When it is required to fit a function with n arbitary constants to a set of m results from an experimental or analytical procedure and n is less than m, then the problem arises of selecting the n points, termed precision points, from the experimental curve required in order to calculate the n constants in the analytical function. One method is to choose the accuracy points by means of the Chebyshev spacing rule.

If f(x) is thought of as the analytic function which truly represents the curve through all of the points and F(x) is the approximating function then the error R(x)

$$R(x) = f(x) - F(x)$$

Now if the error R(x) is expressed as

$$R(x) = G(x-t_1)\ (x-t_2)\ \ldots\ldots(x-t_n)$$

Where t_1 t_2 etc., are the accuracy points. The requirement that the error will be a minimum is satisfied if the maximum and mimimum of R(x) are all of equal magnitude and alternate between the accuracy points. The form of R(x) to give this condition, and hence the accuracy points, is given by a class of polynomials known as the Chebyshev polynomials, the roots of which give t_1 t_2 etc. A simple graphical method exists for finding those roots. From the mid point of the range of x draw a circle of radium one-half of the internal and inscribe a polygon of 2n sides with two of its sides perpendicular to the axis of x. The projections of the Vertices of the polygon onto the x axis determine the accuracy points. The construction for n = 2 is shown in Figure 11.

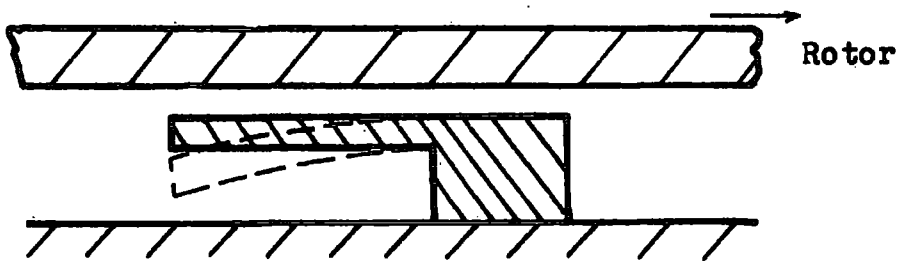

The "Cantilever" thrust pad.

Figure 1.

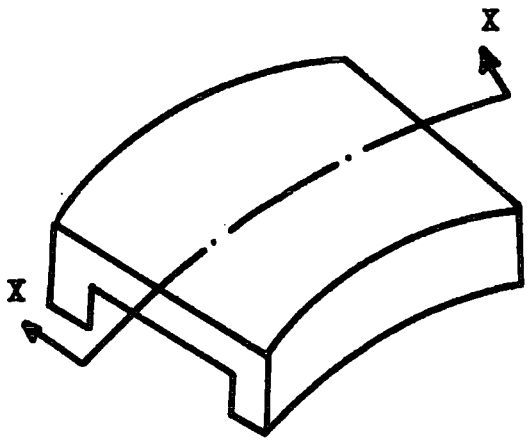

(a)

(b) (c)

The 'diaphram' thrust pad.

Figure 2.

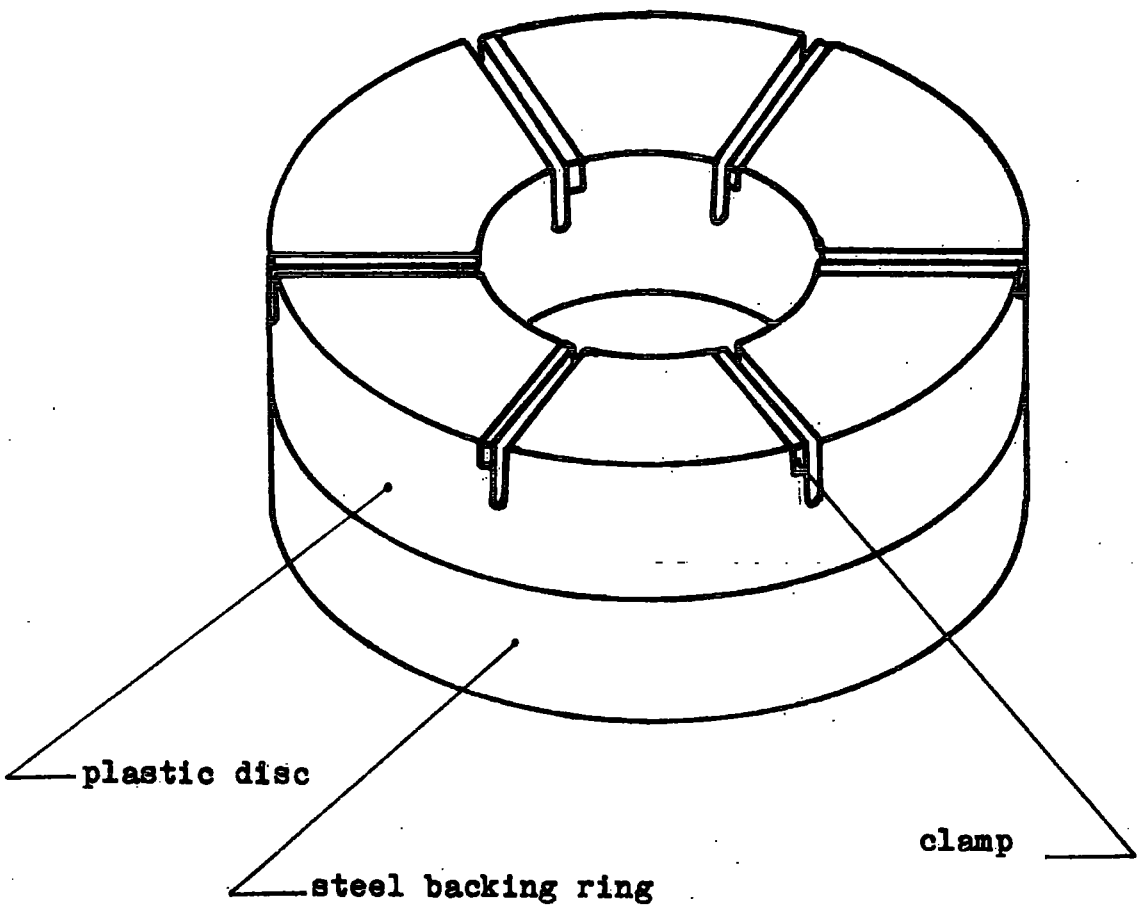

The 'compliant' thrust pad.

Figure 3.

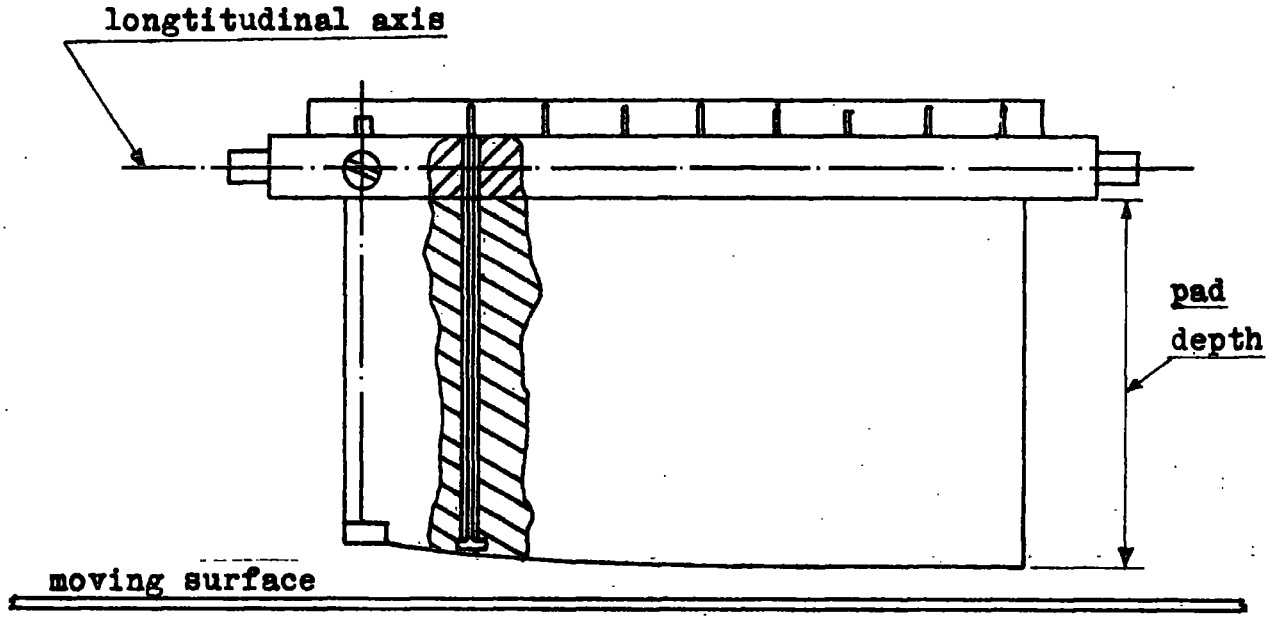

Schematic diagram of final pad form
with the deflection probes.

Fig. 4

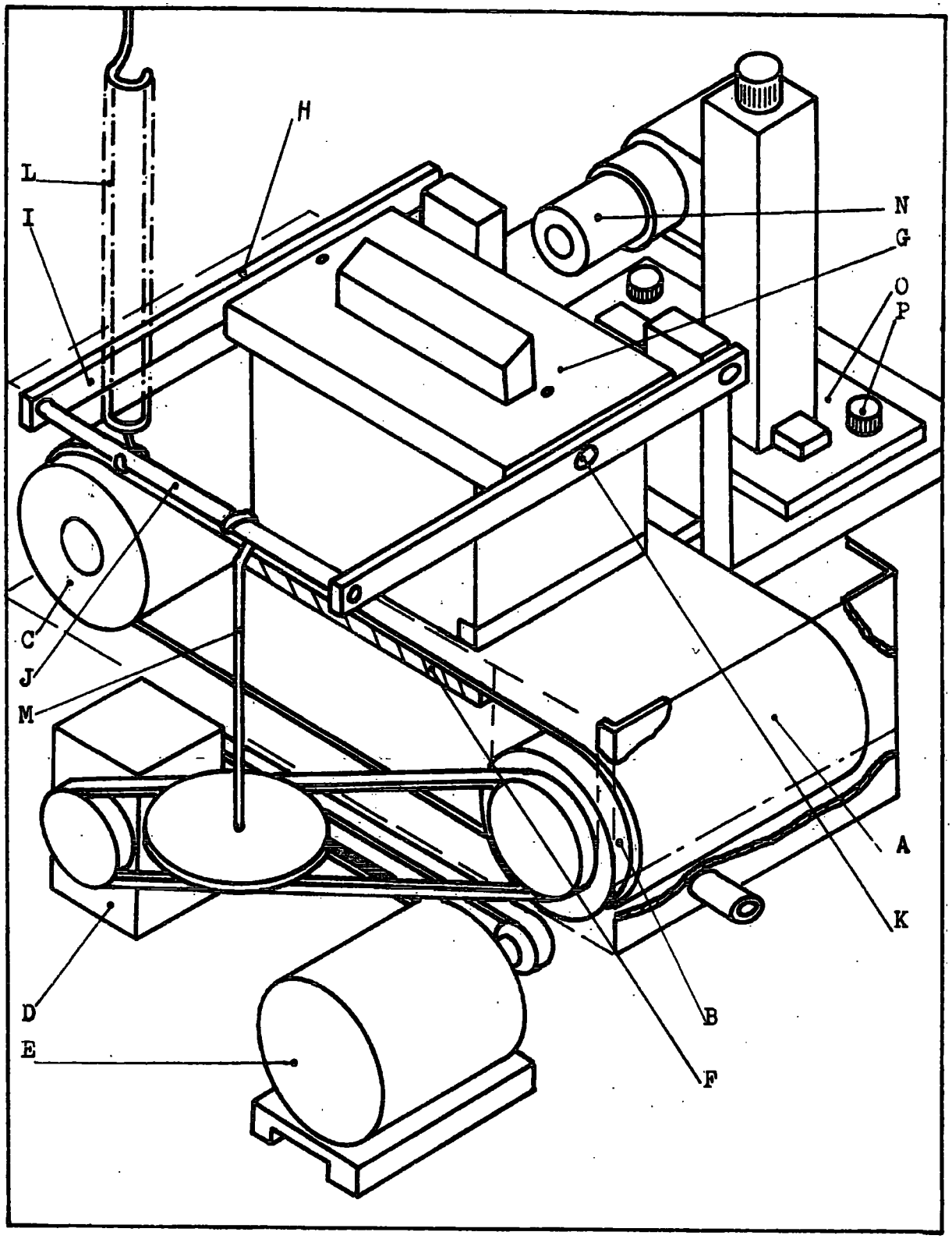

The Test rig assembly. Schematic diagram.

Figure 5.

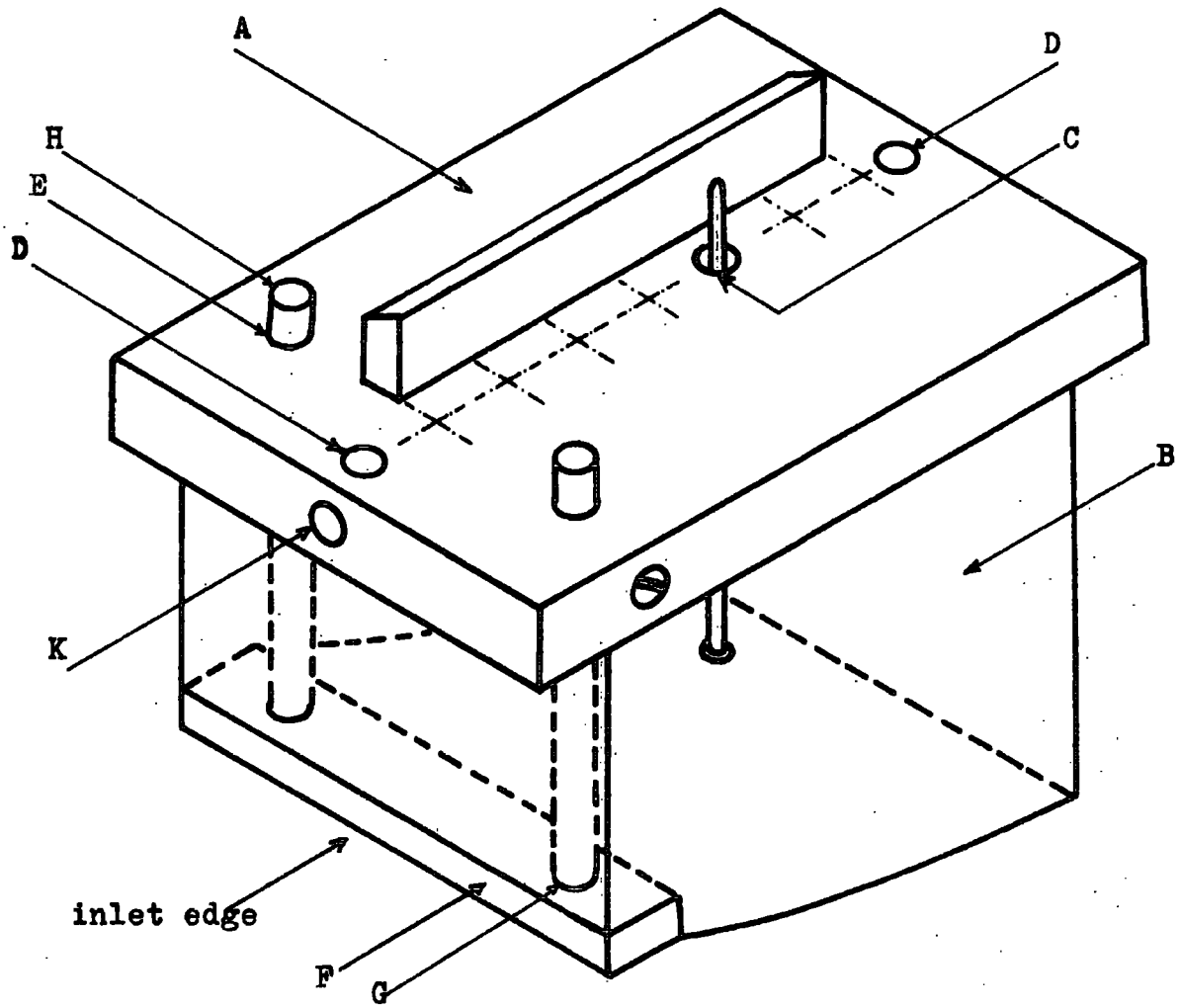

The pad assembly.

Figure 6.

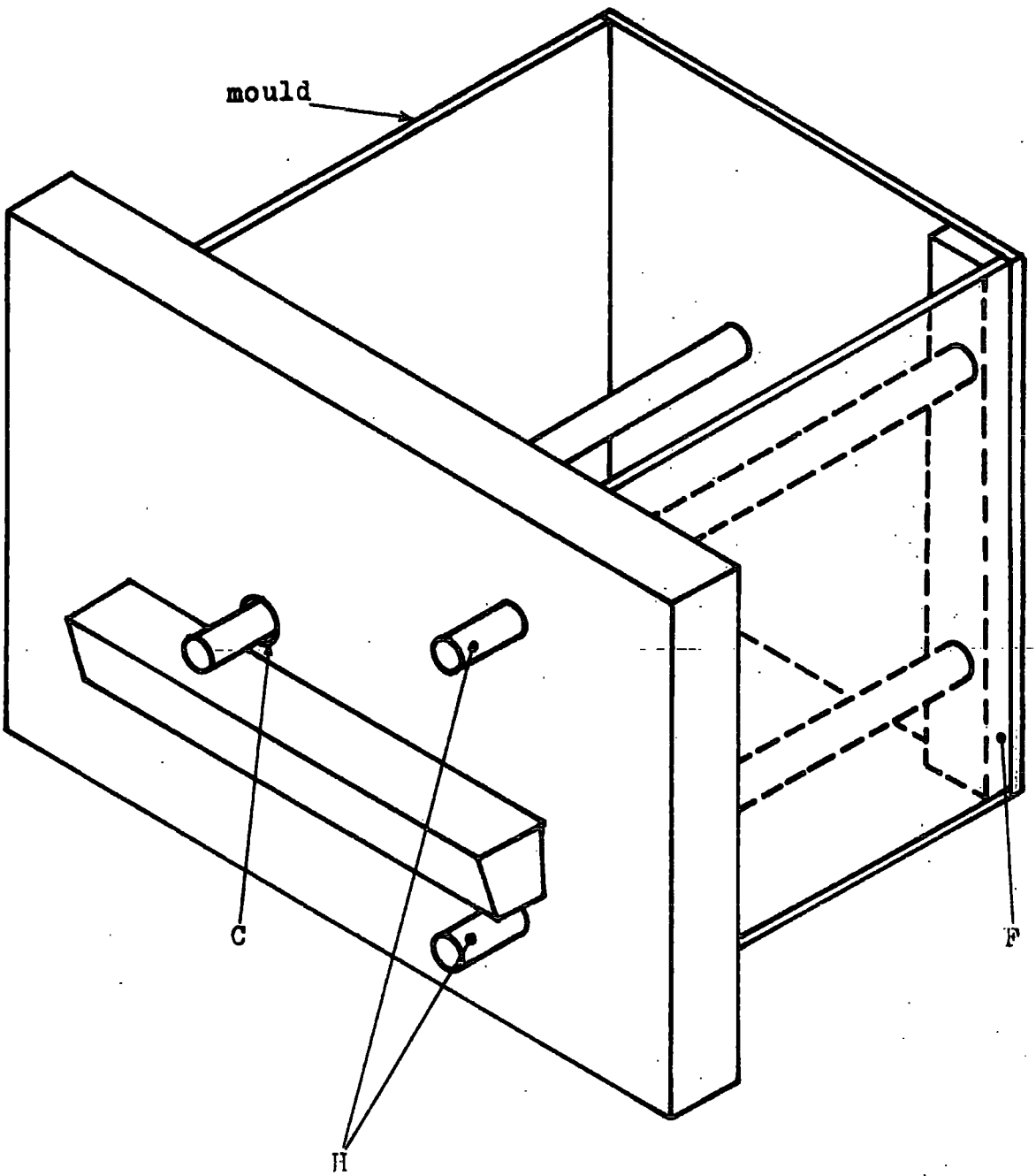

The pad mould. Stage I.
Figure 7.

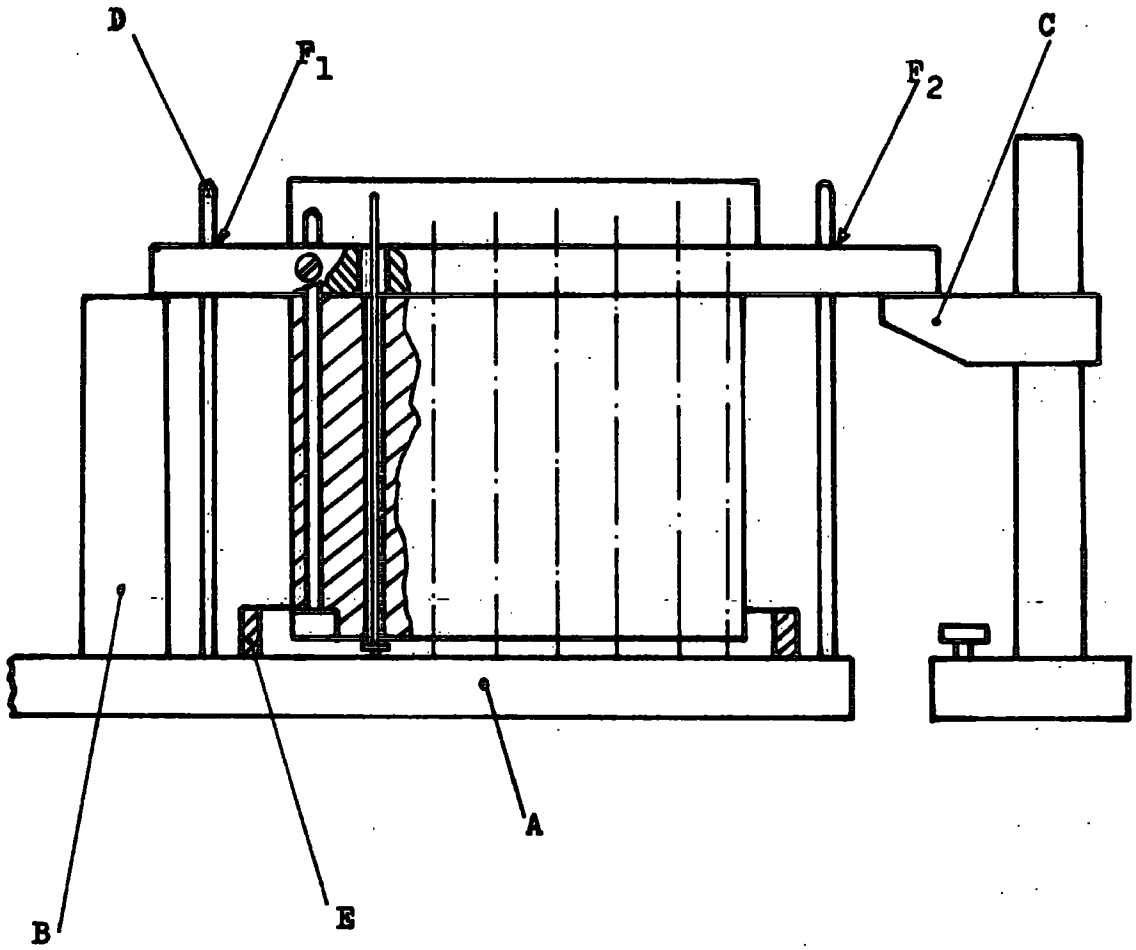

The pad set-up for moulding. Stage II.

Figure 8.

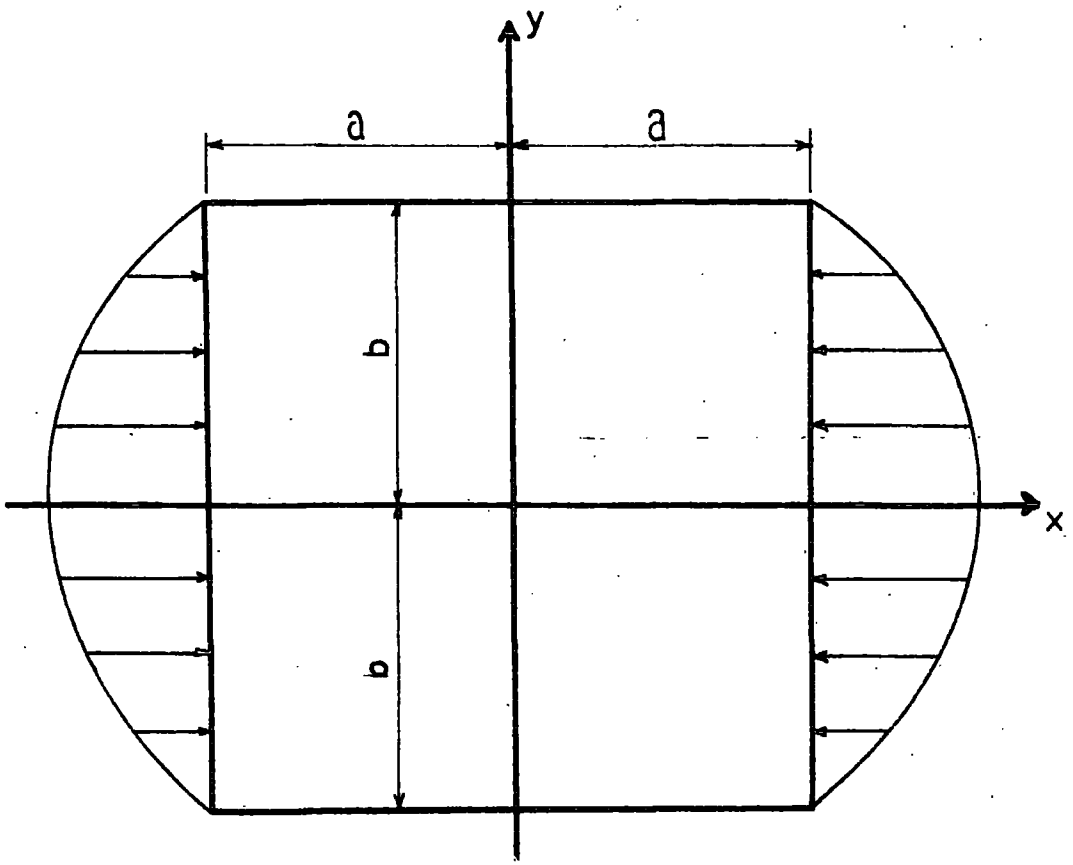

Model for the stress analysis.

Figure 9.

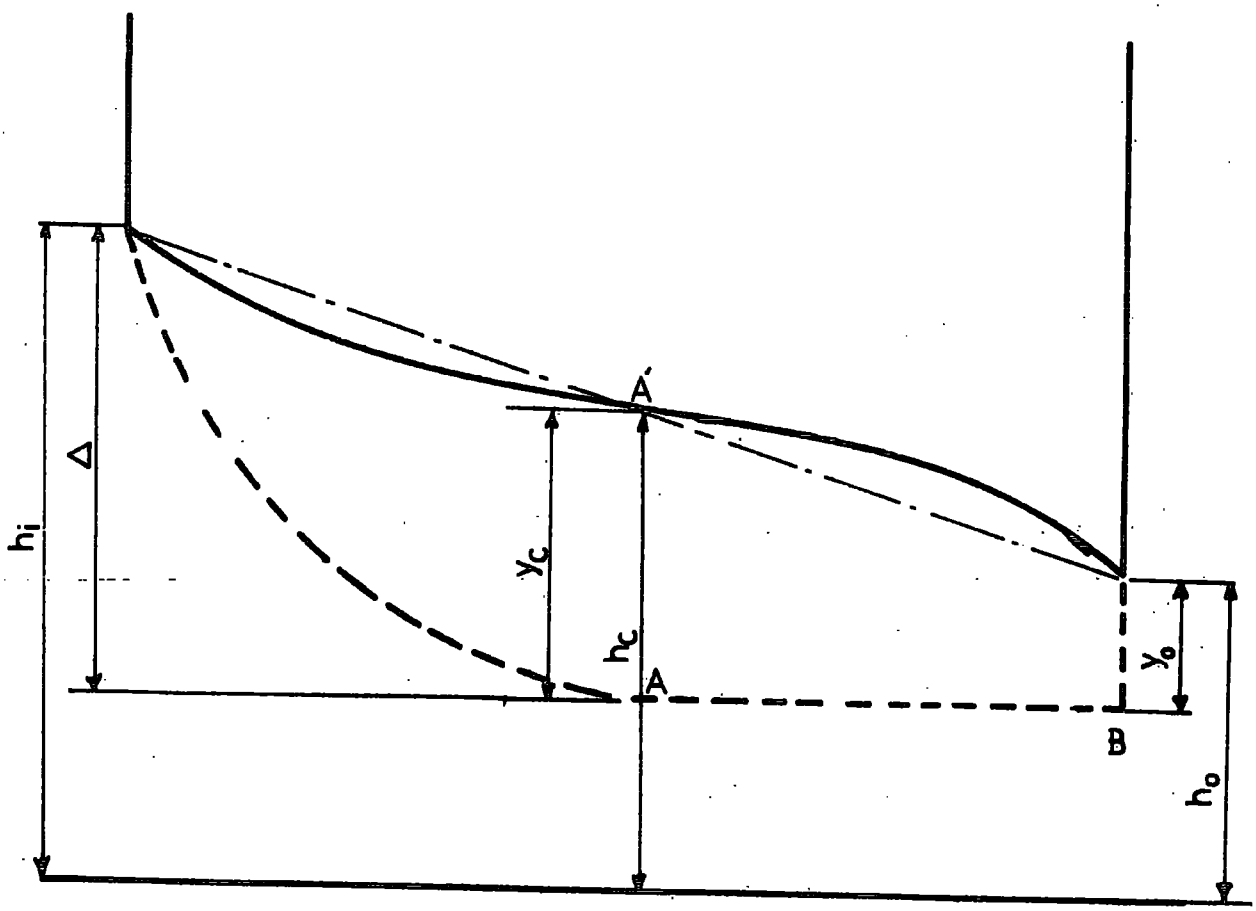

The model for the critical pressure no. estimation.

Figure 10.

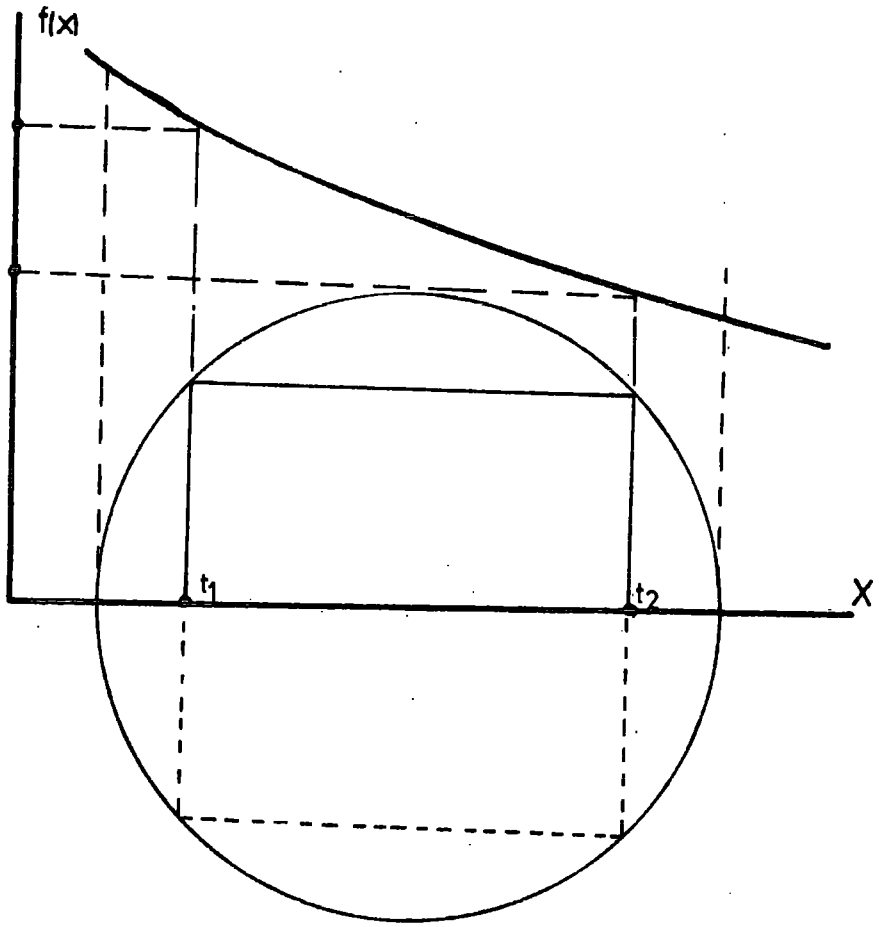

Example of Chebyshev spacing applied to two accuracy points

Figure 11.

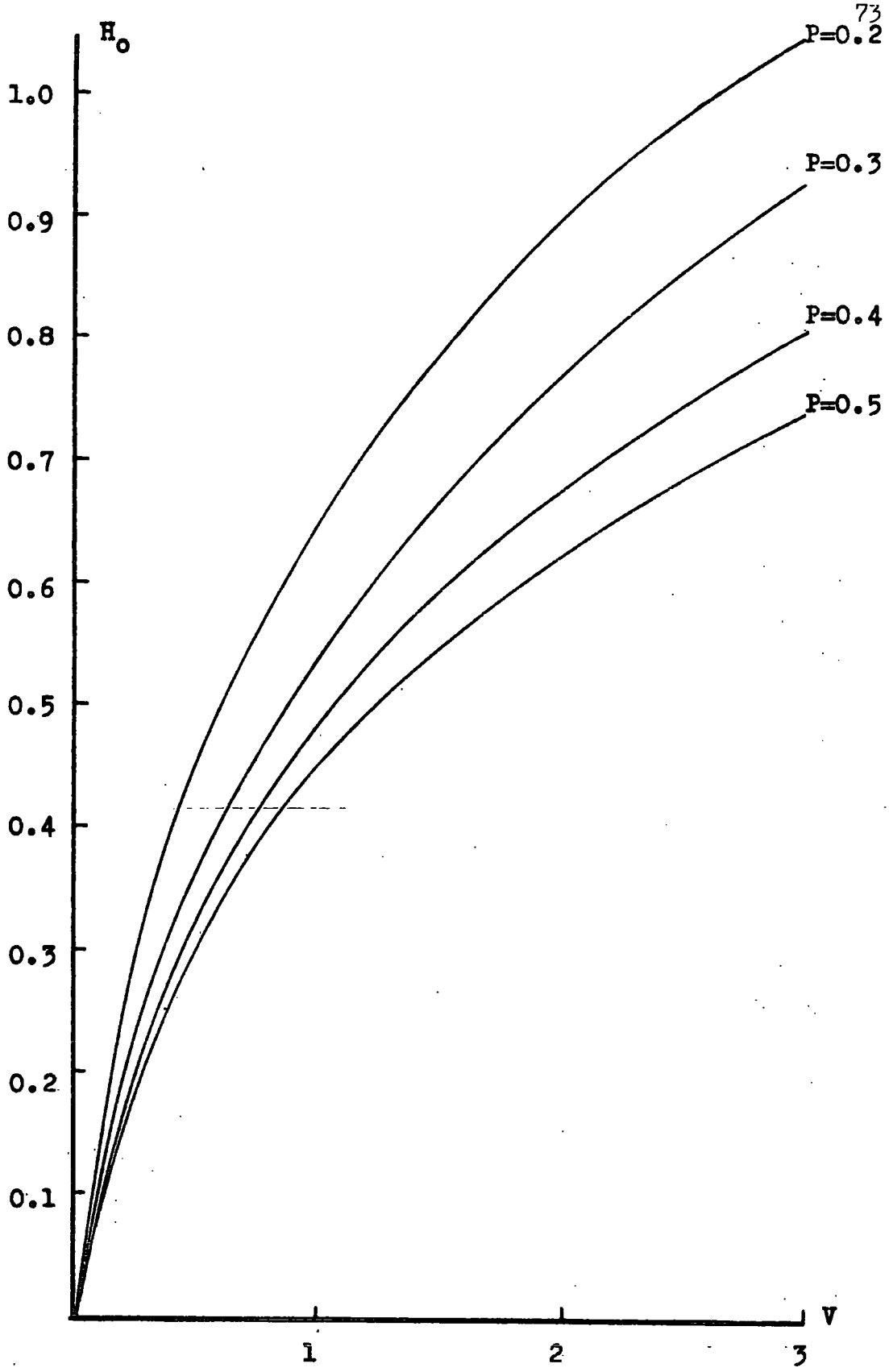

Variation of the film thickness no. with velocity no.

Graph 4.o

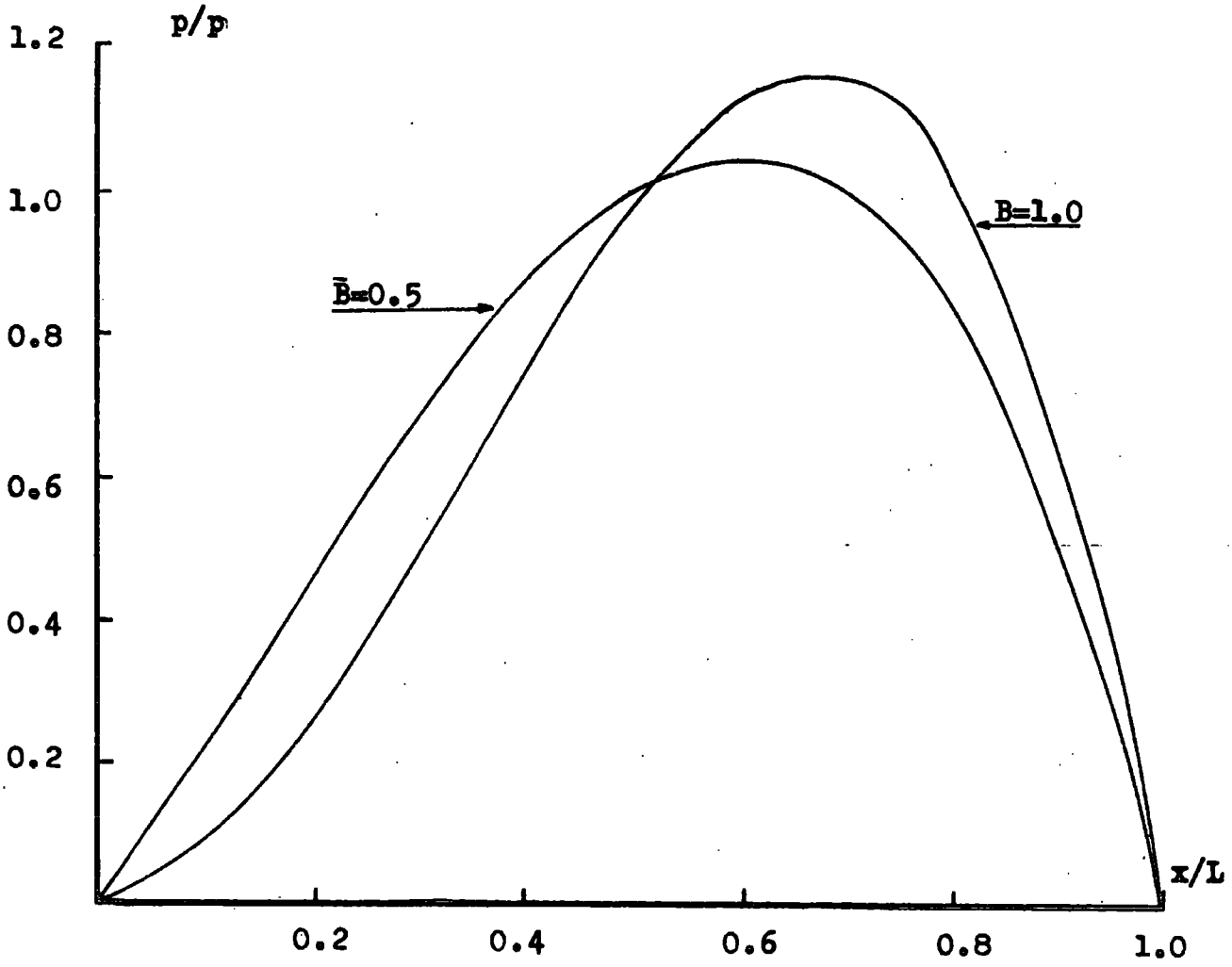

The assumed pressure profile for the stress analysis.

Graph 4.1

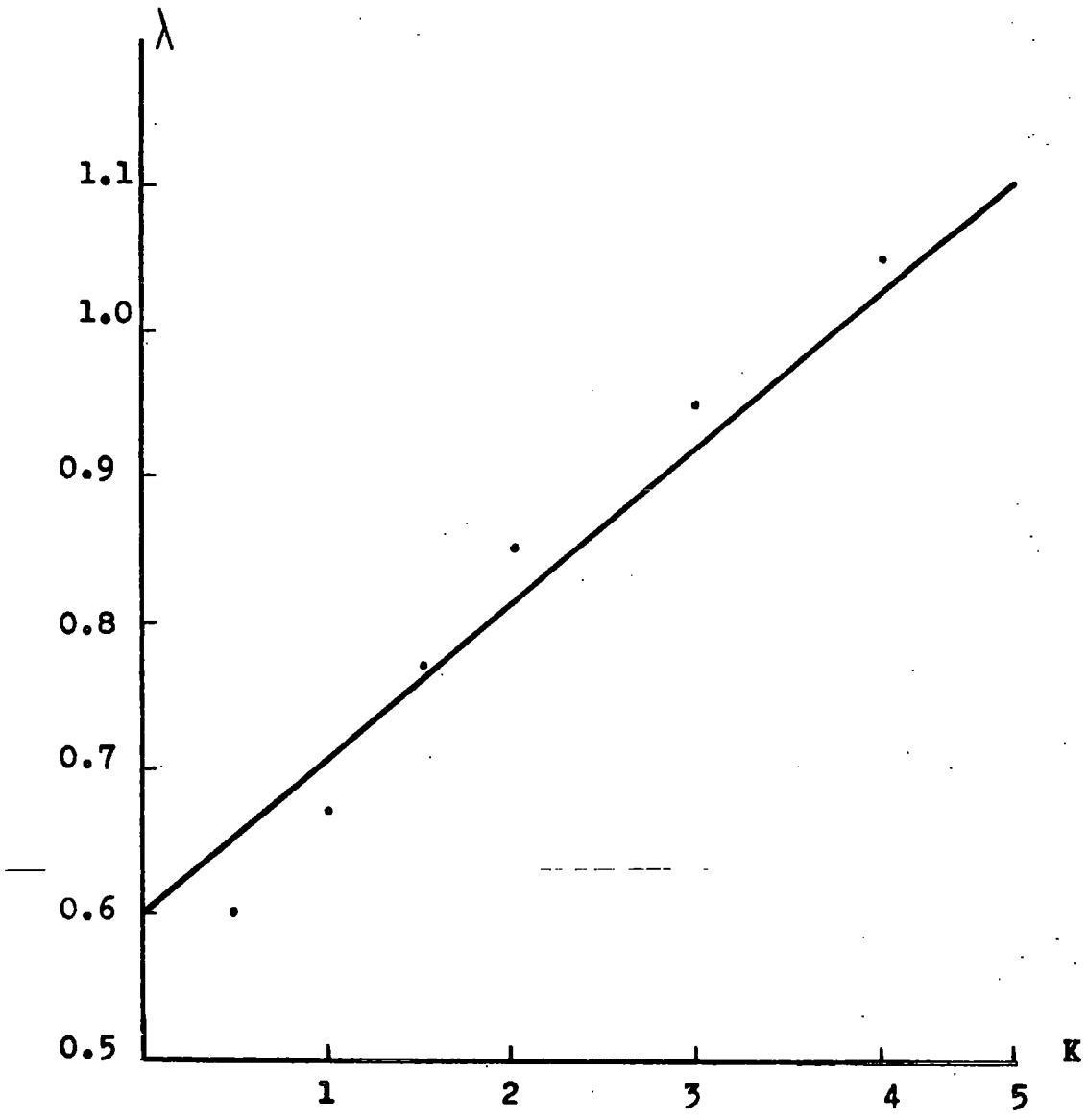

Variation in the deflection coeficient with the pad inclination.

Graph 4.2

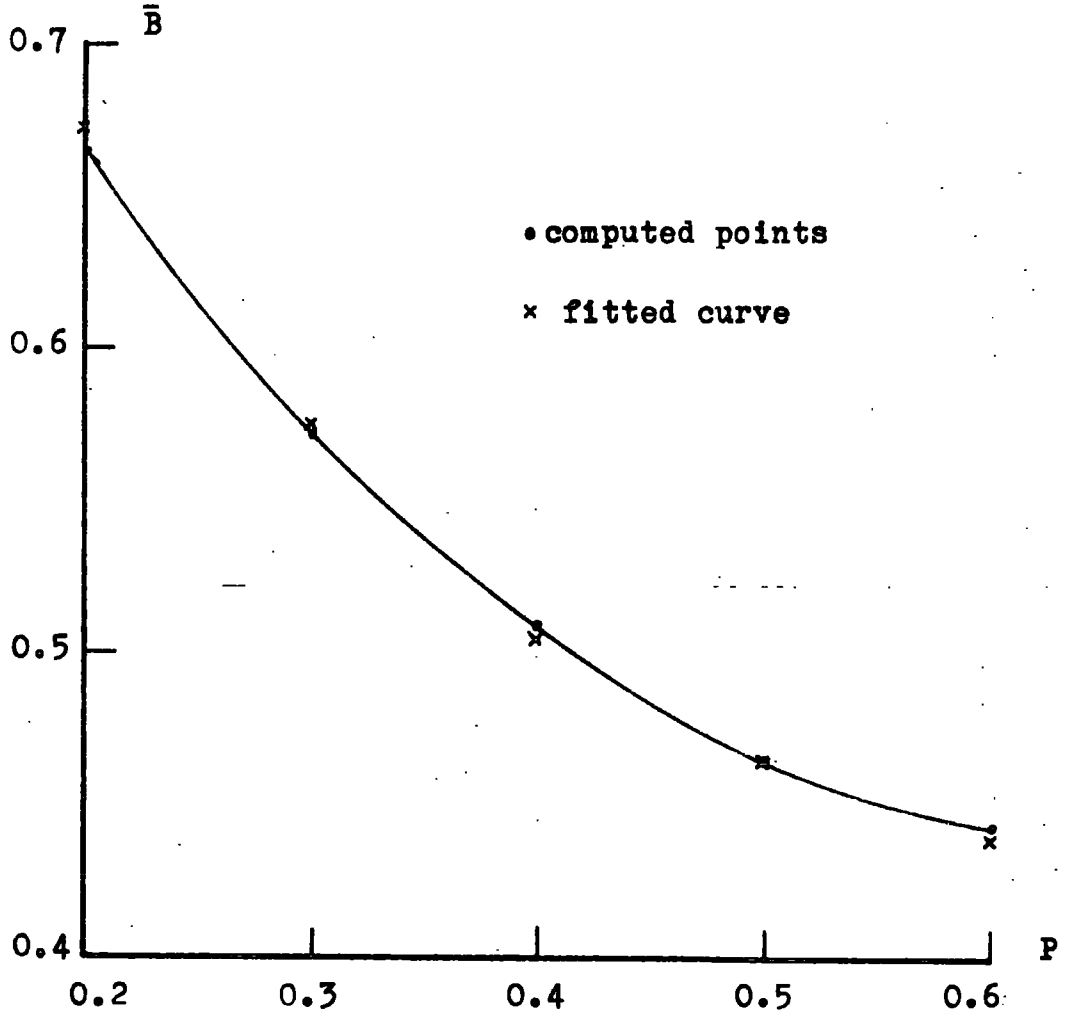

Variation of $\bar{B}$ with the pressure no. P

Graph 4.3

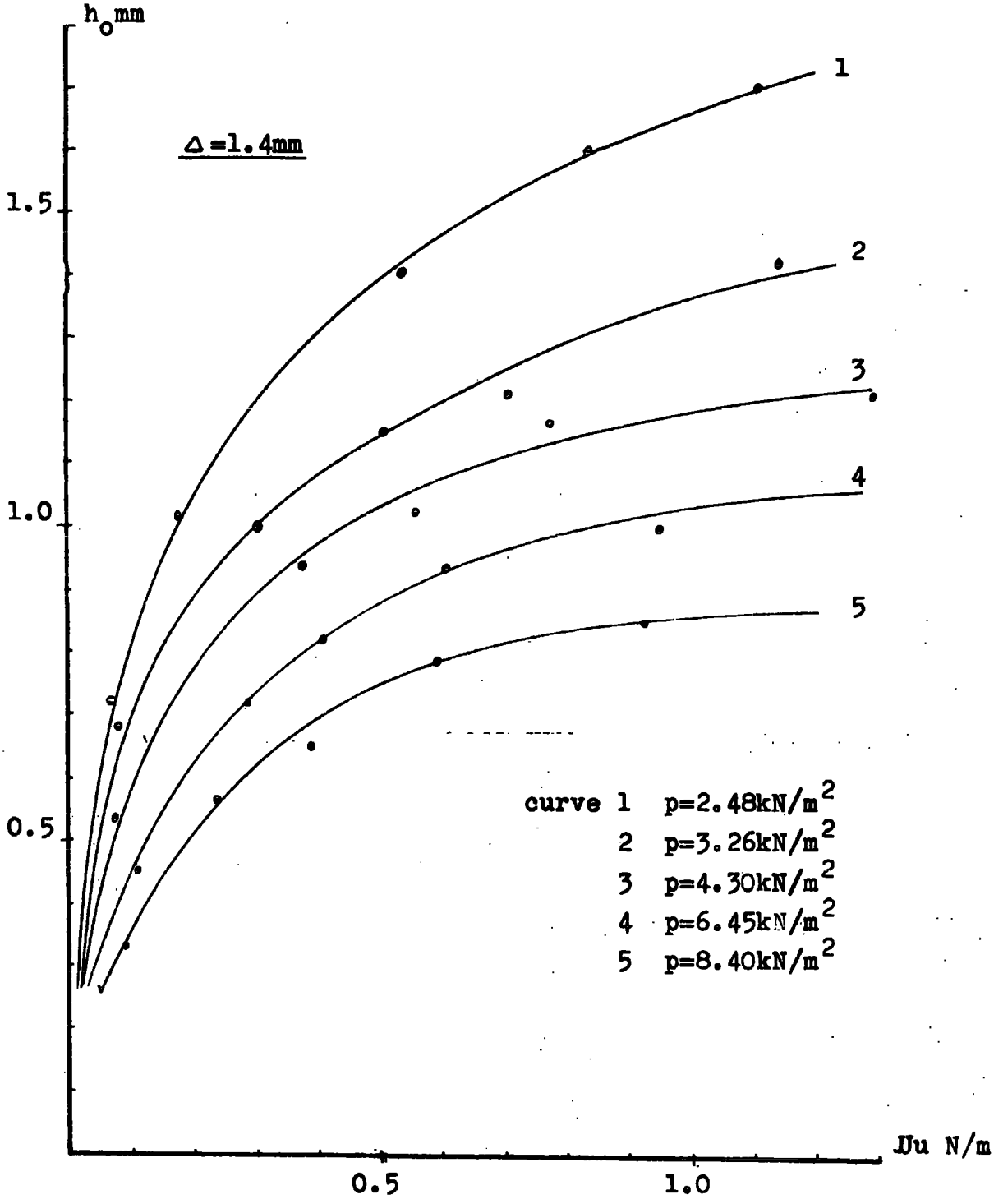

Variation in outlet film thickness with belt velocity.
Constant load curves.

Graph 5.0

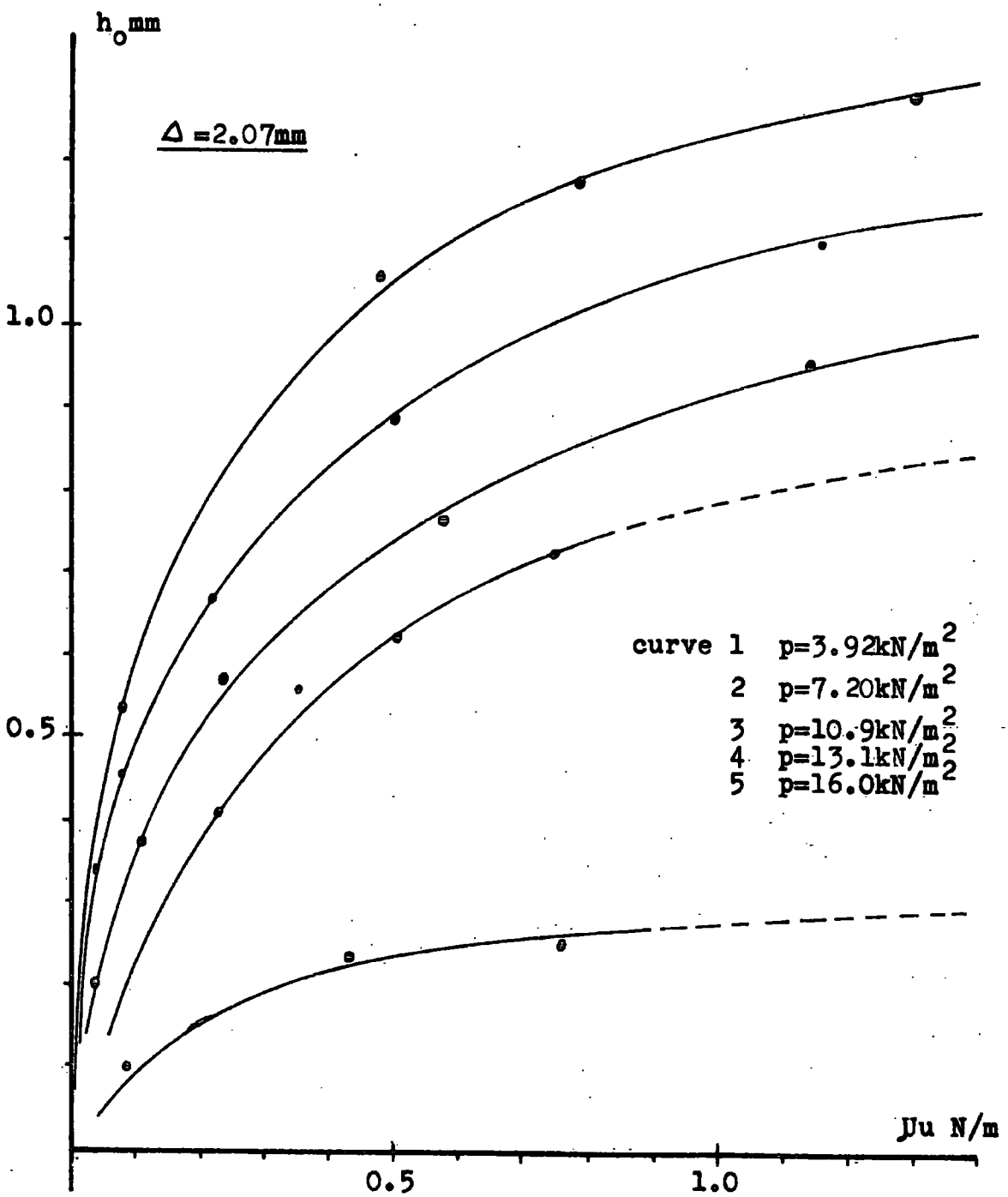

Variation in outlet film thickness with belt velocity.
Constant load curves.

Graph 5.1

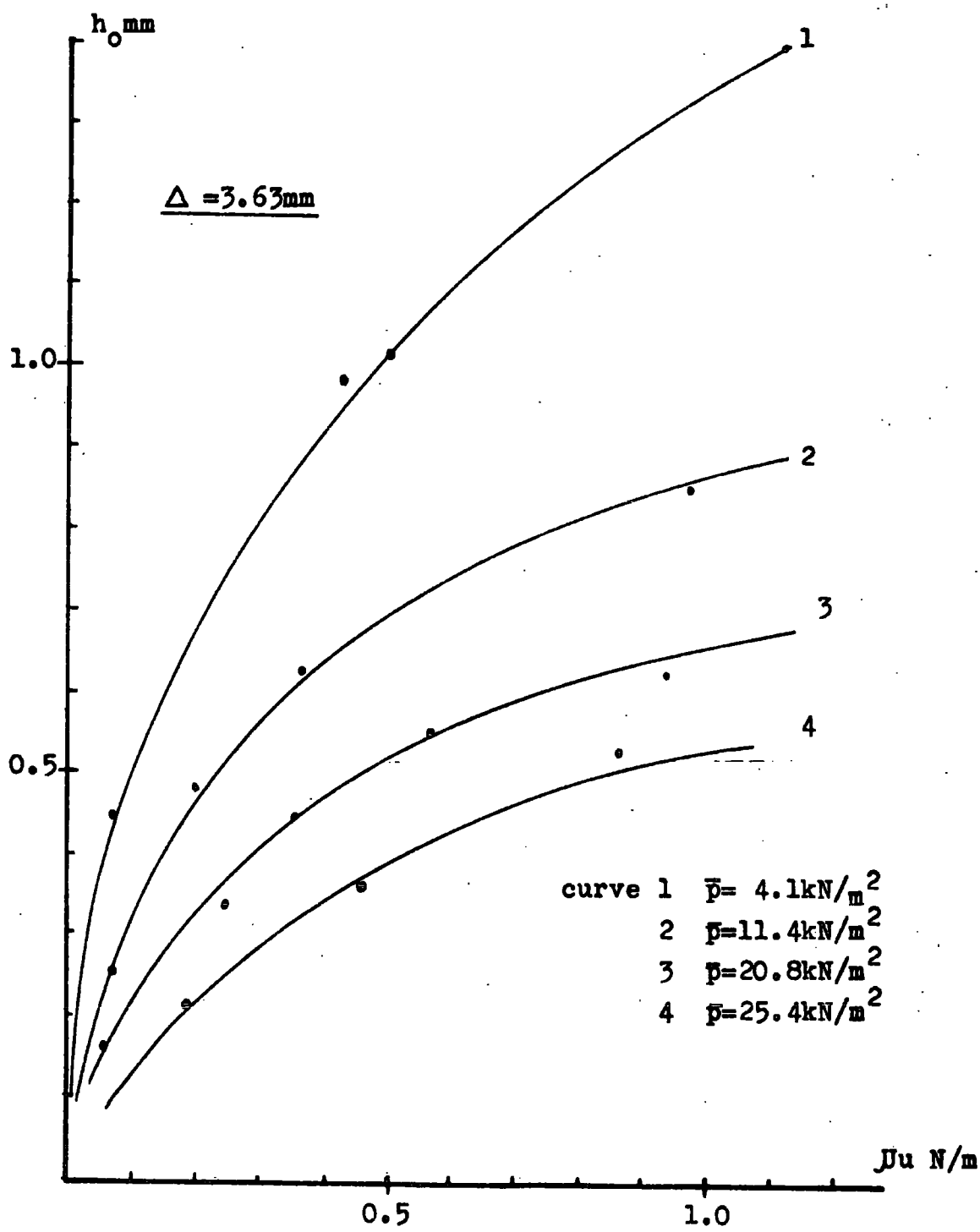

Variation in outlet film thickness with belt velocity.
Constant load curves.

Graph 5.2

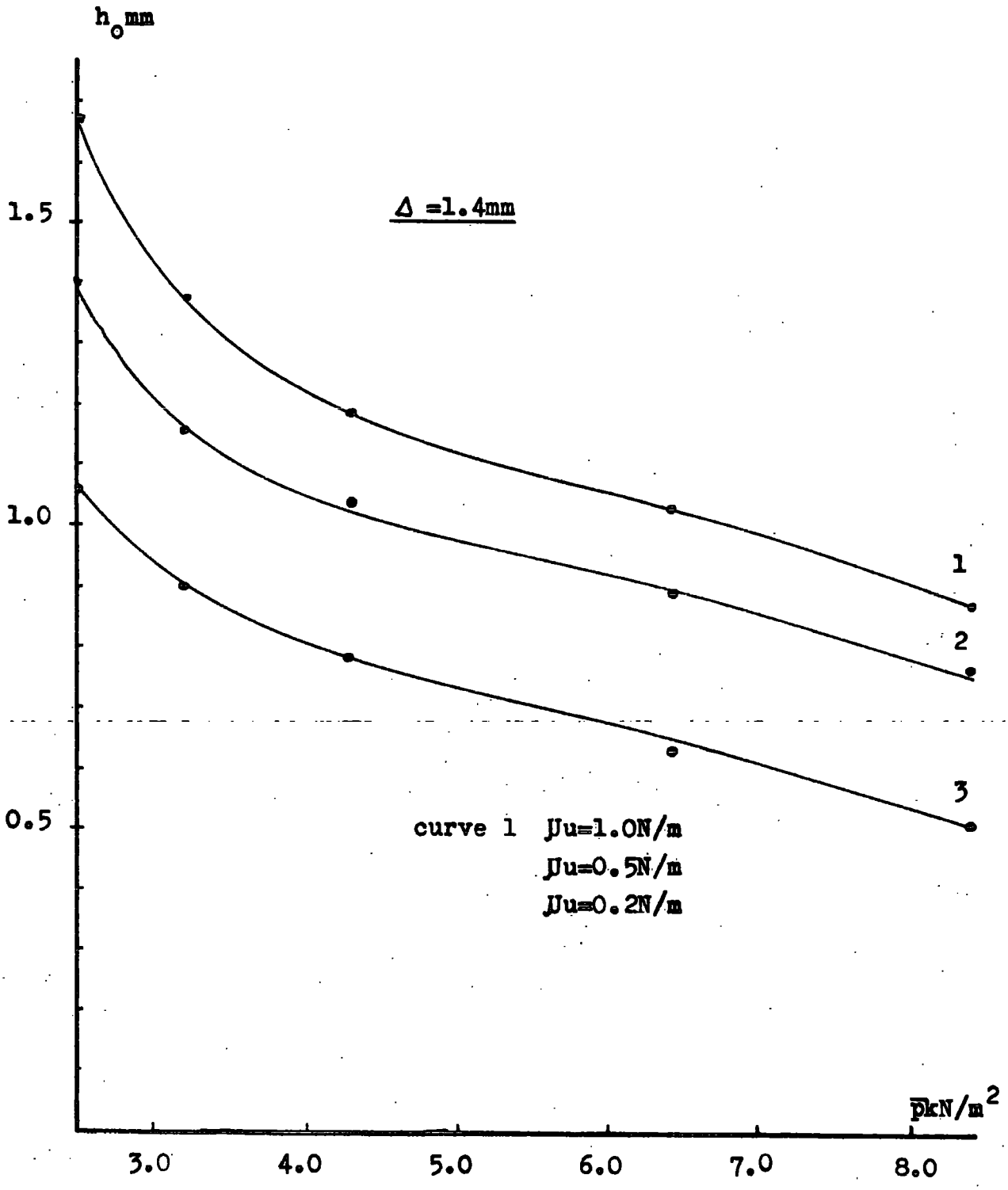

Variation in outlet film thickness with mean applied pressure.
Curves of constant velocity

Graph 5.3

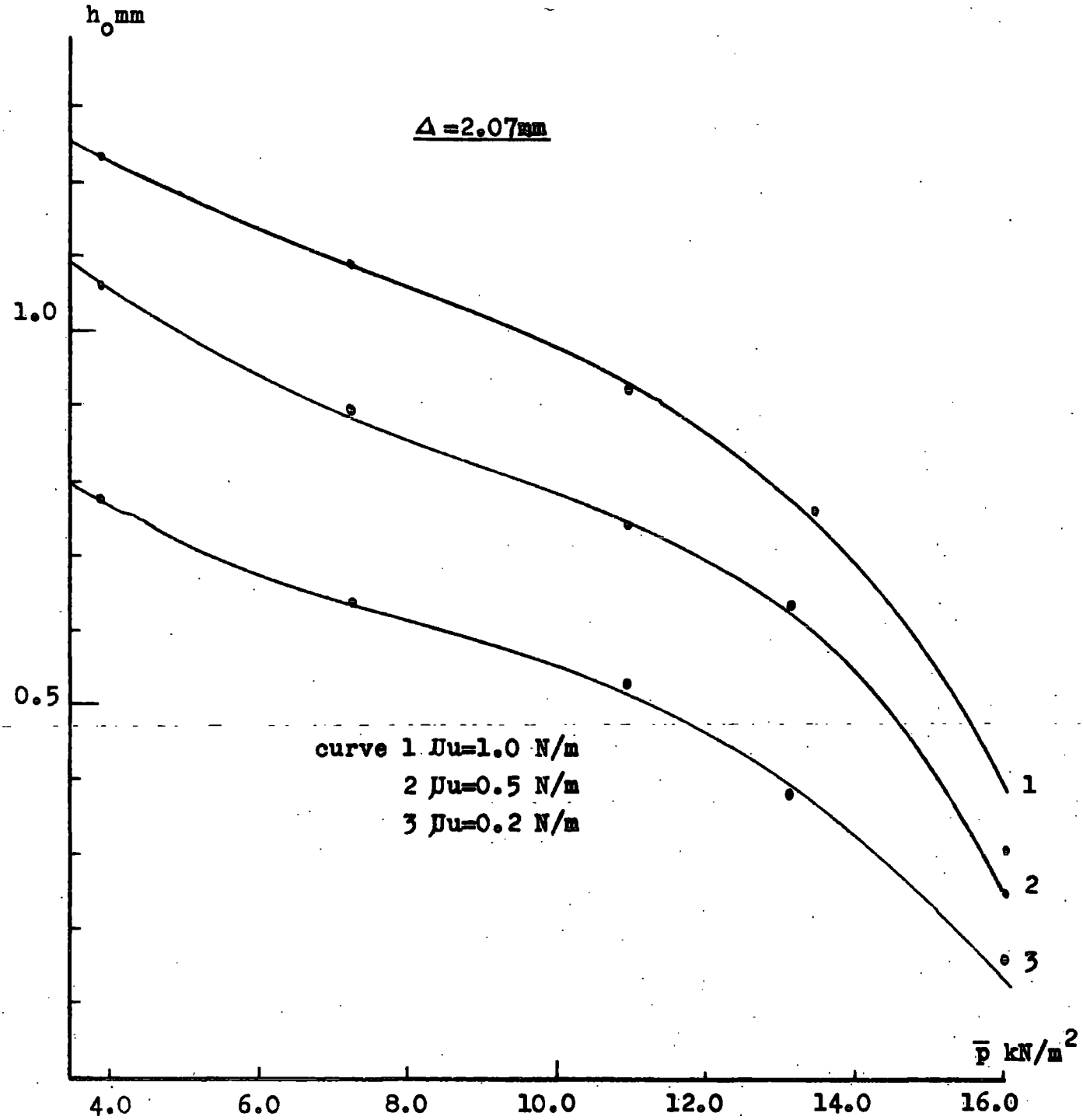

Variation in outlet film thickness with mean applied pressure.
Curves of constant velocity.

Graph 5.4

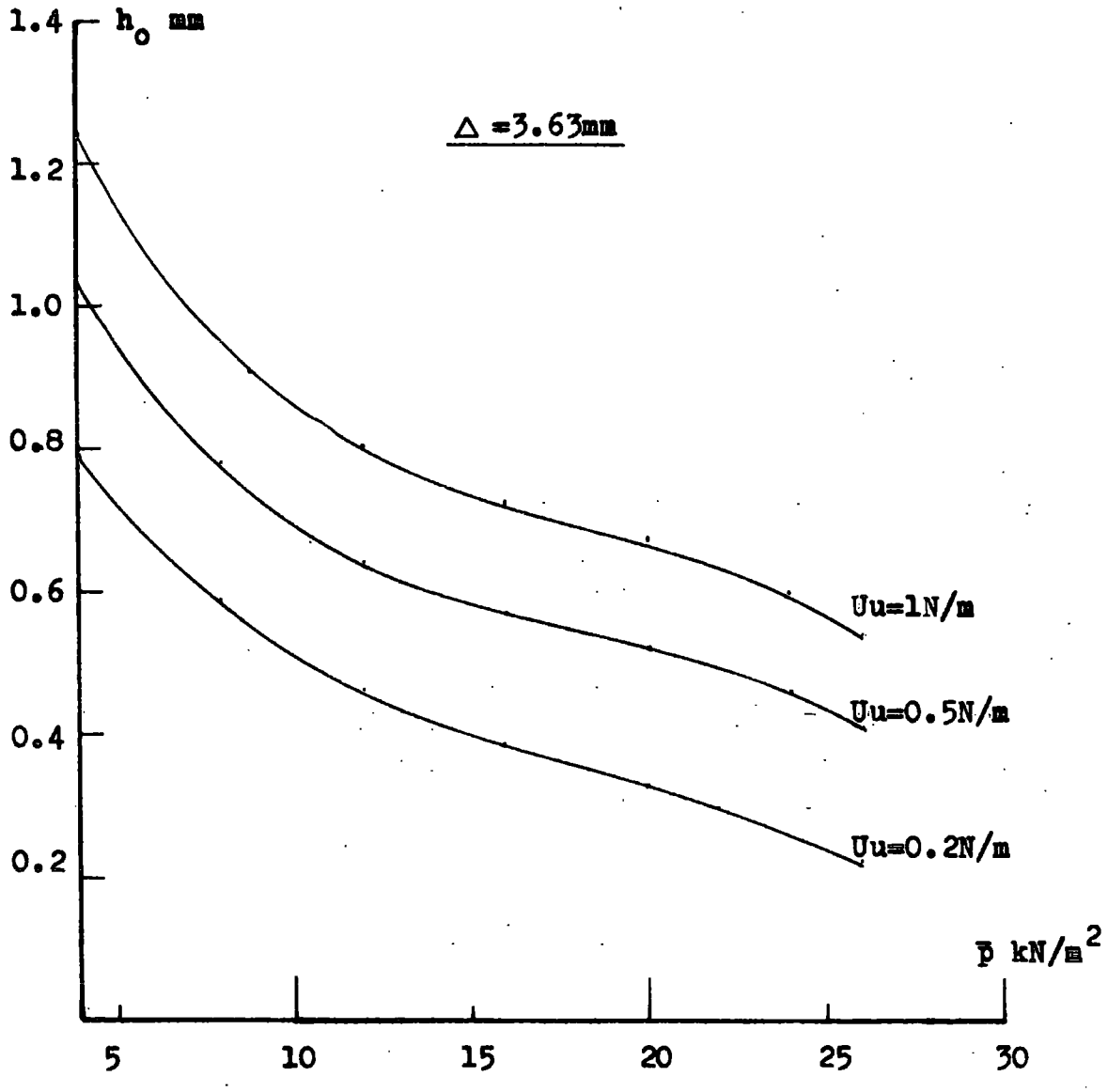

Variation in outlet film thickness with mean applied pressure.

Curves of constant velocity.

Graph 5.5

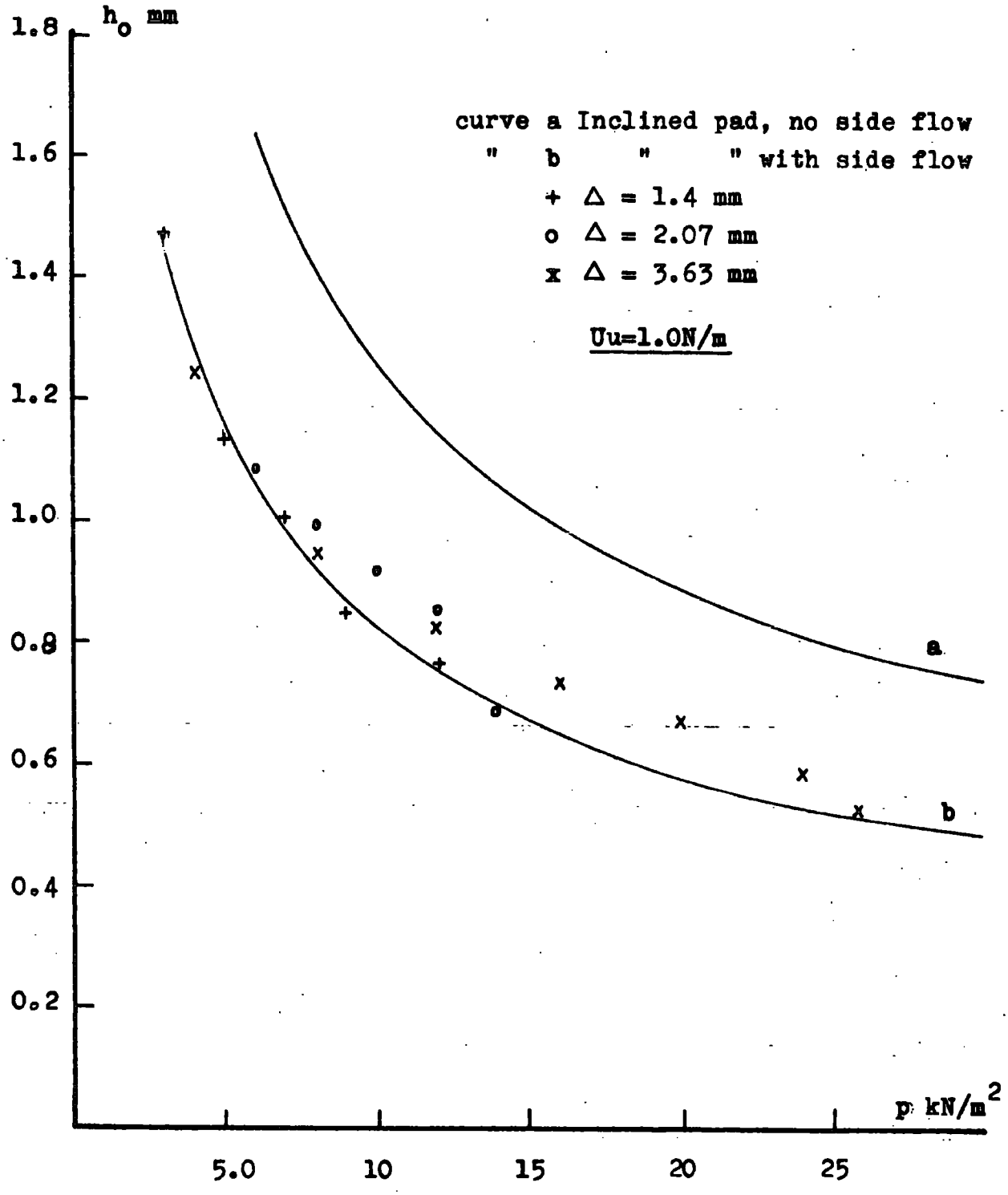

Comparison between the compliant pad and the flat inclined pad of optimum slope.

Curves of constant velocity.

Graph 5.6

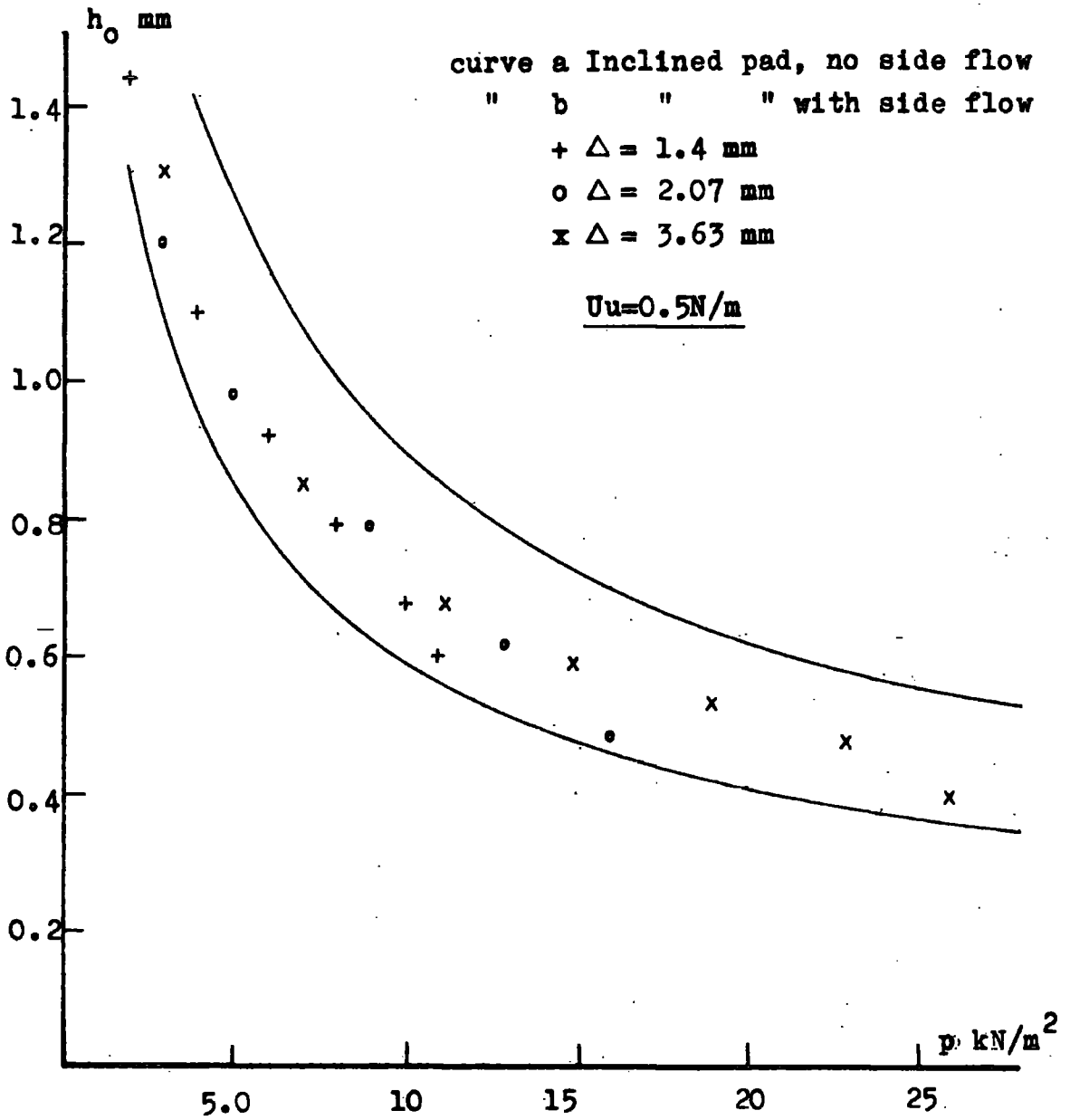

Comparison between the compliant pad and the flat inclined pad of optimum slope.

Curves of constant velocity.

Graph 5.7

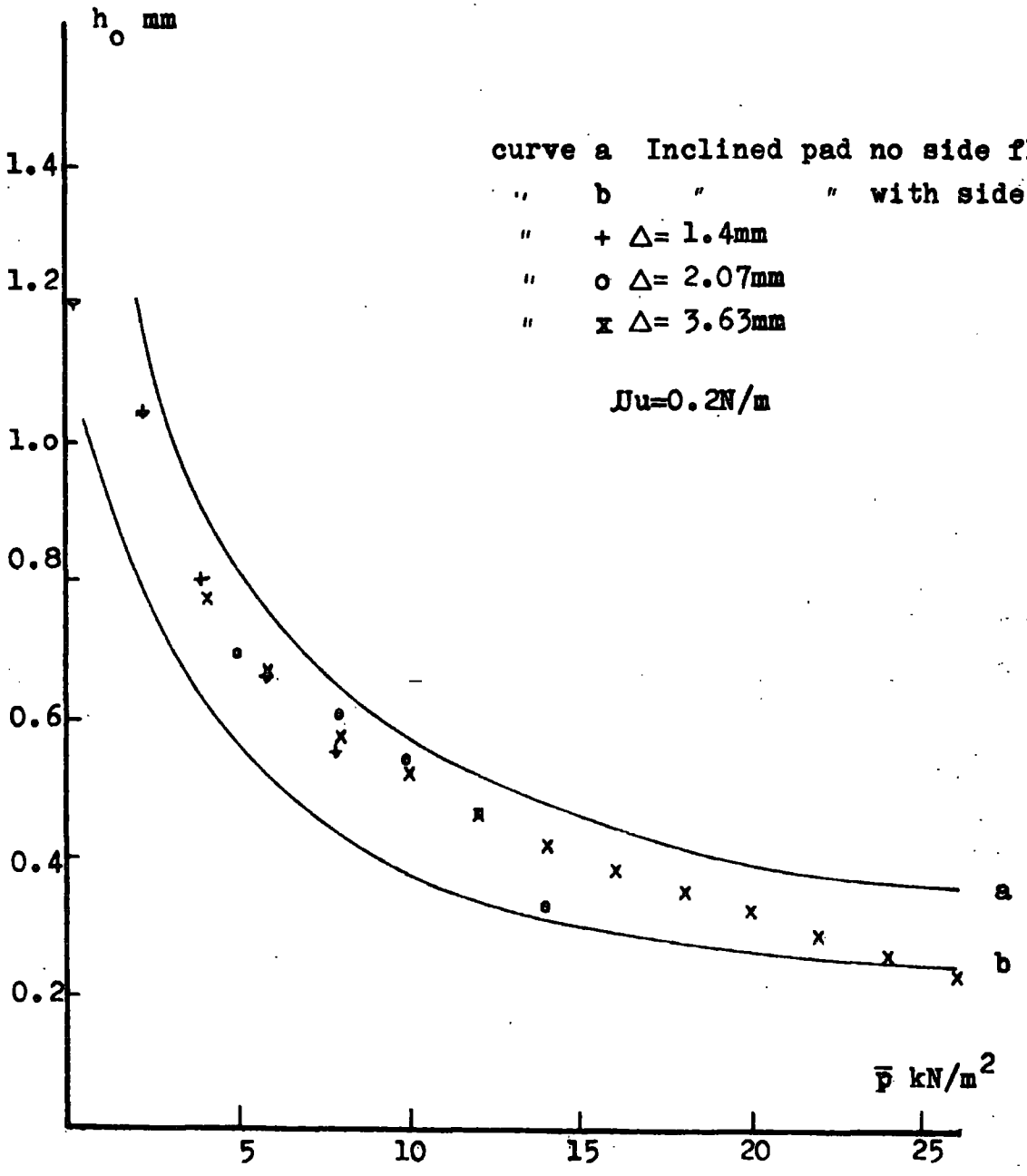

Comparison between the compliant pad and the flat inclined pad of optimum slope.

Curves of constant velocity.

Graph 5.8

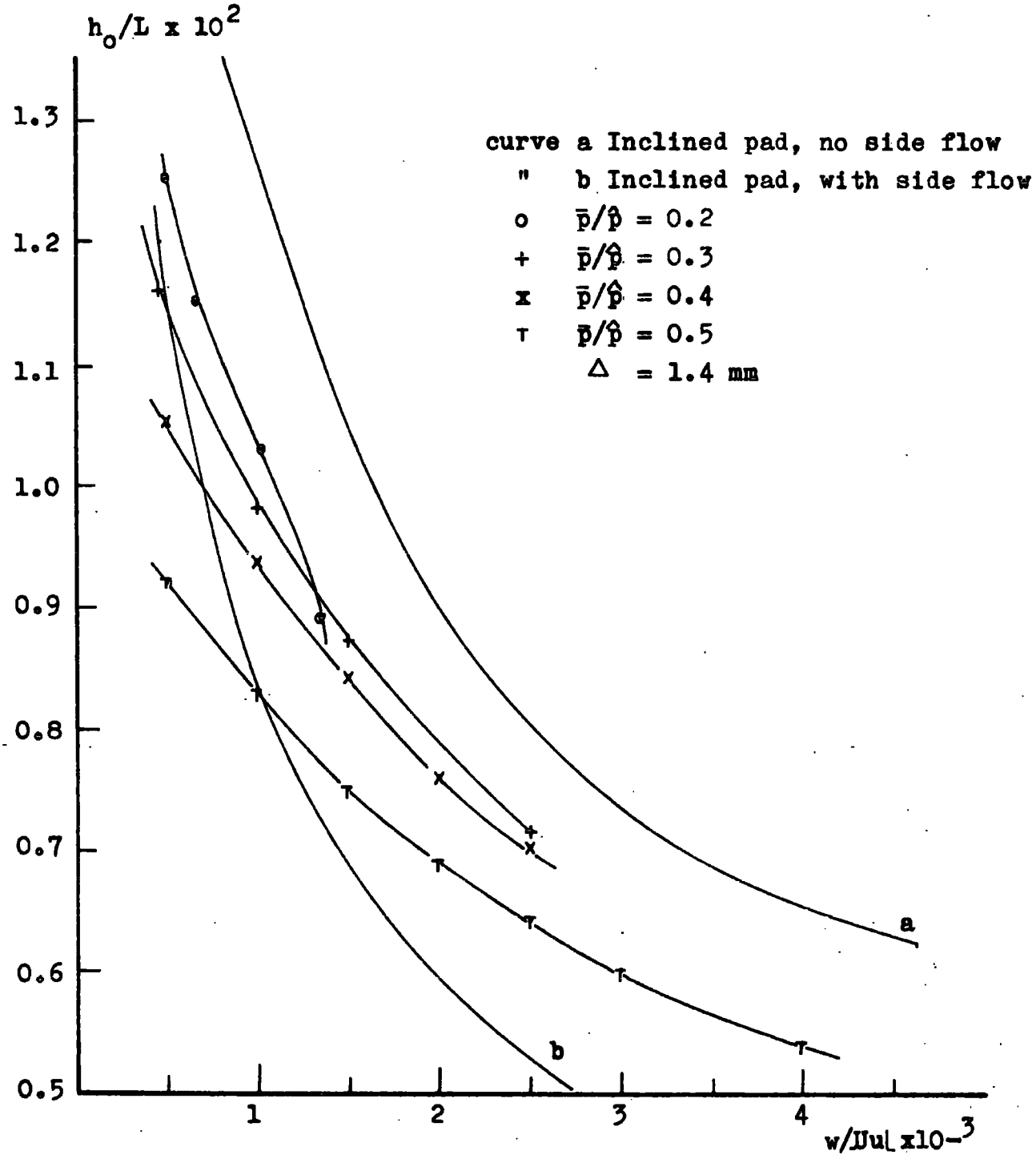

Non-dimensional film thickness against a duty parameter
Curves of constant mean pressure

Graph 5.9

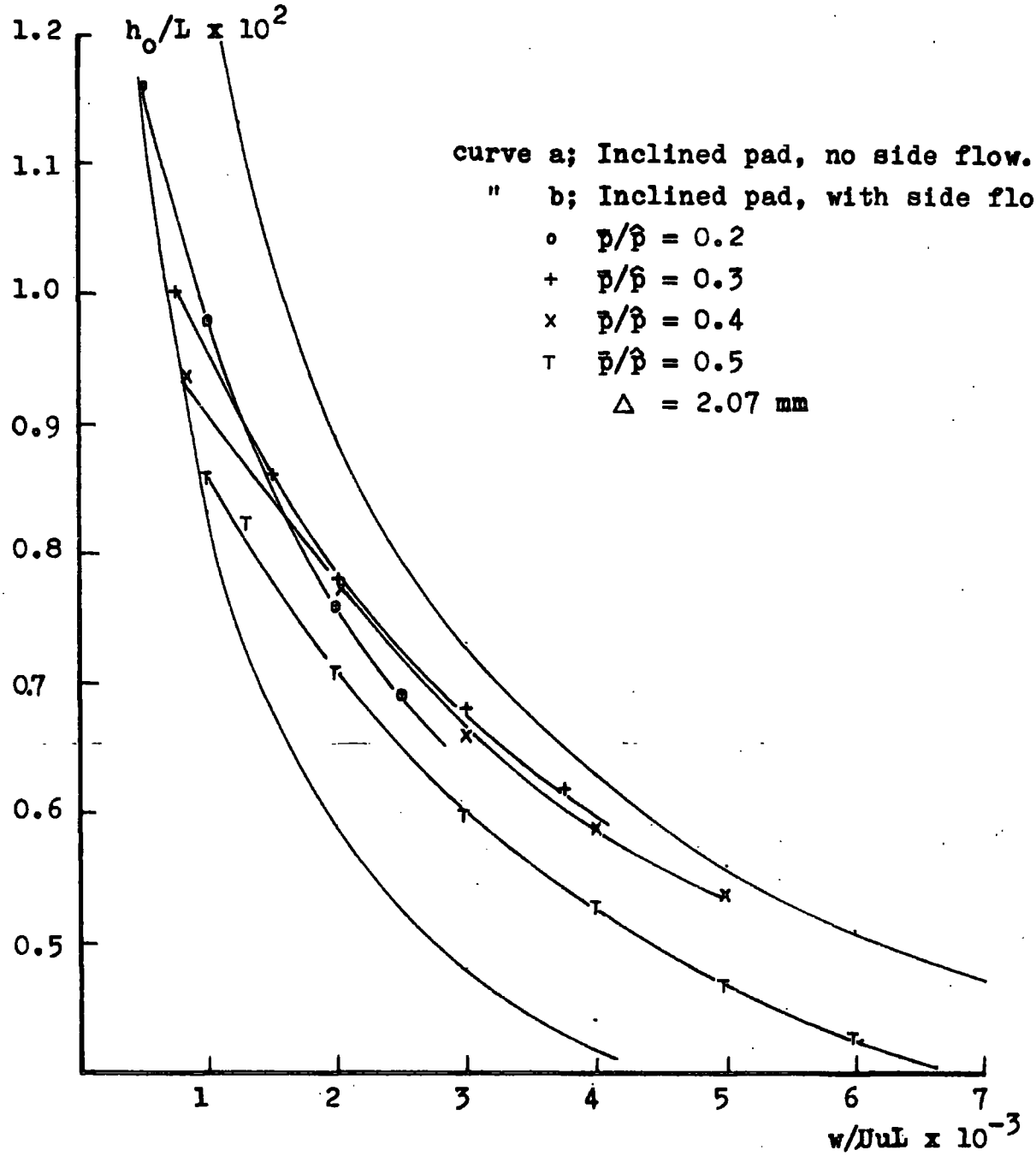

Non-dimensional film thickness against a duty parameter
Curves of constant mean pressure

Graph 5.10

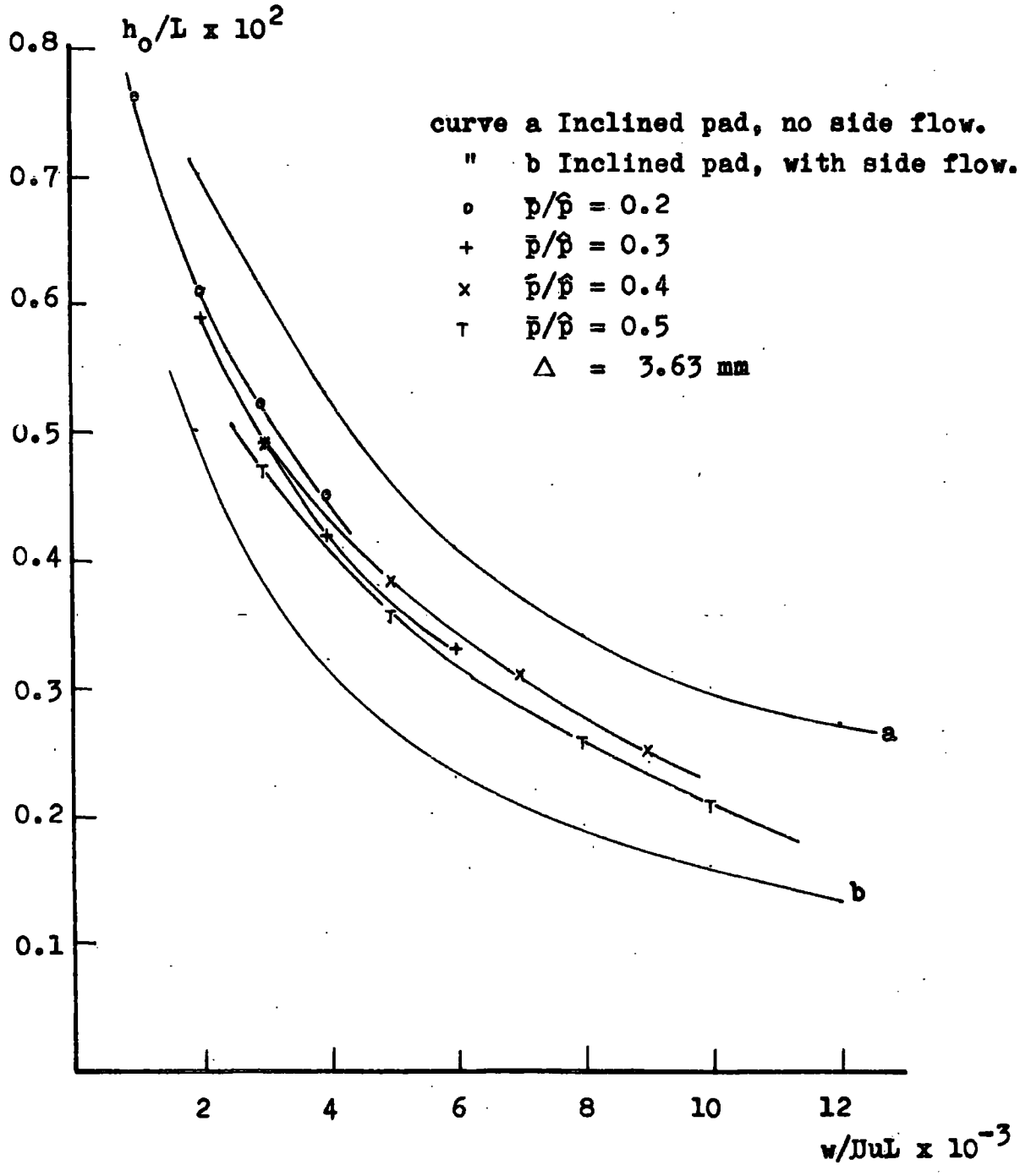

Non-dimensional film thickness against a duty parameter
Curves of constant mean pressure

Graph 5.11

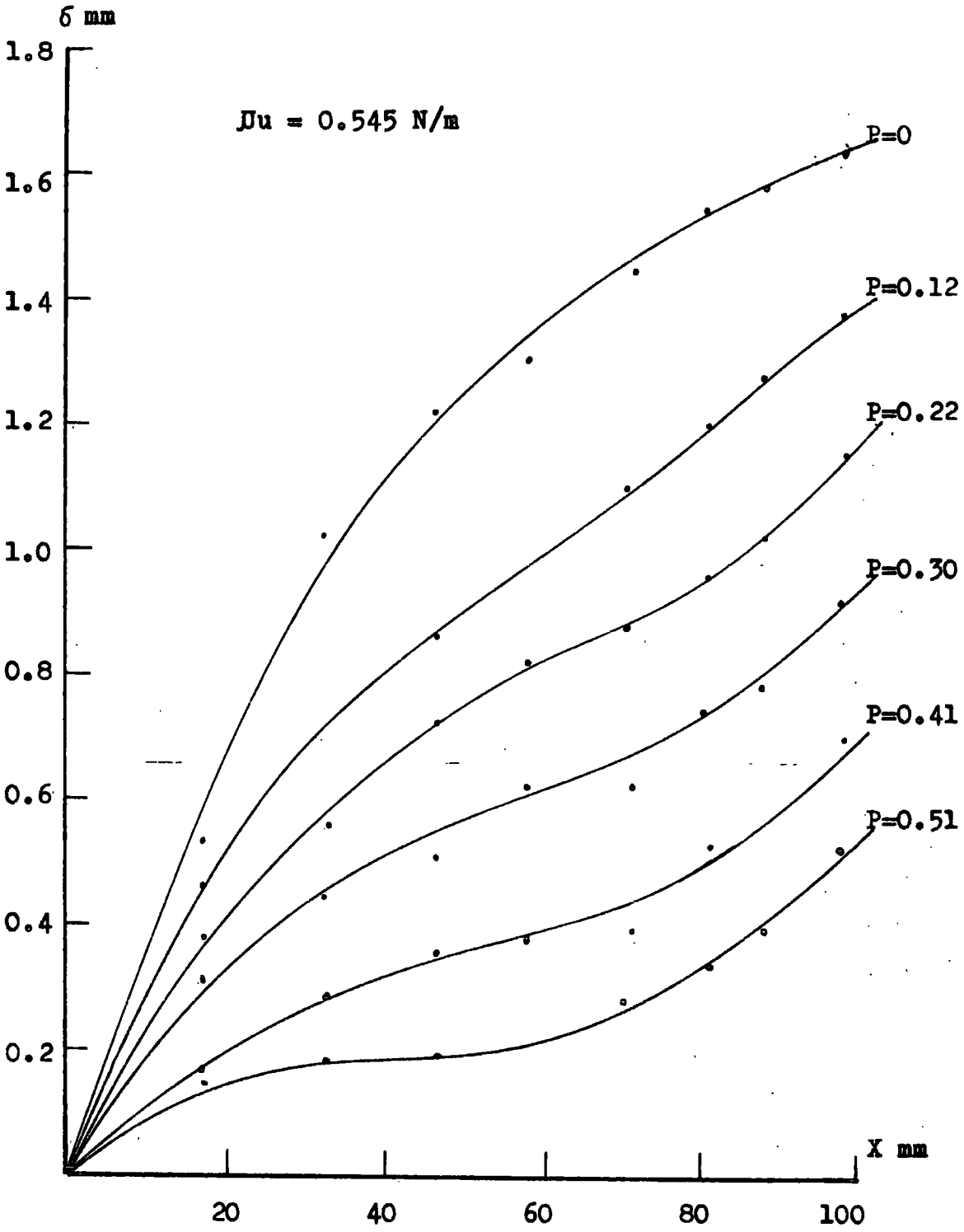

Pad profile.

Graph 5.12

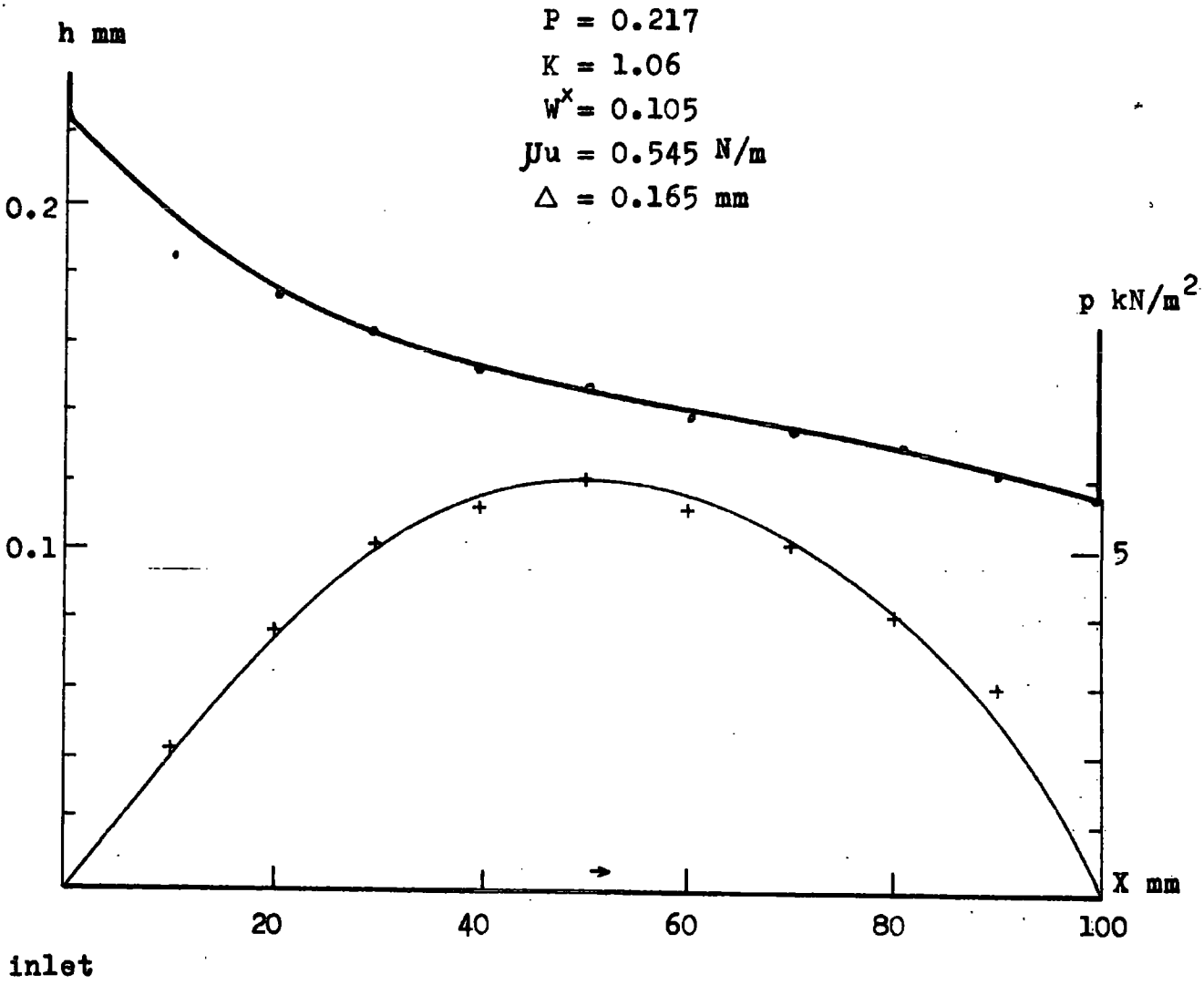

Variation in film thickness and pressure along the pad.

Graph 5.13a

P = 0.302
K = 0.94
W^x = 0.12
$\bar{J}u$ = 0.545 N/m
Δ = 0.165 mm

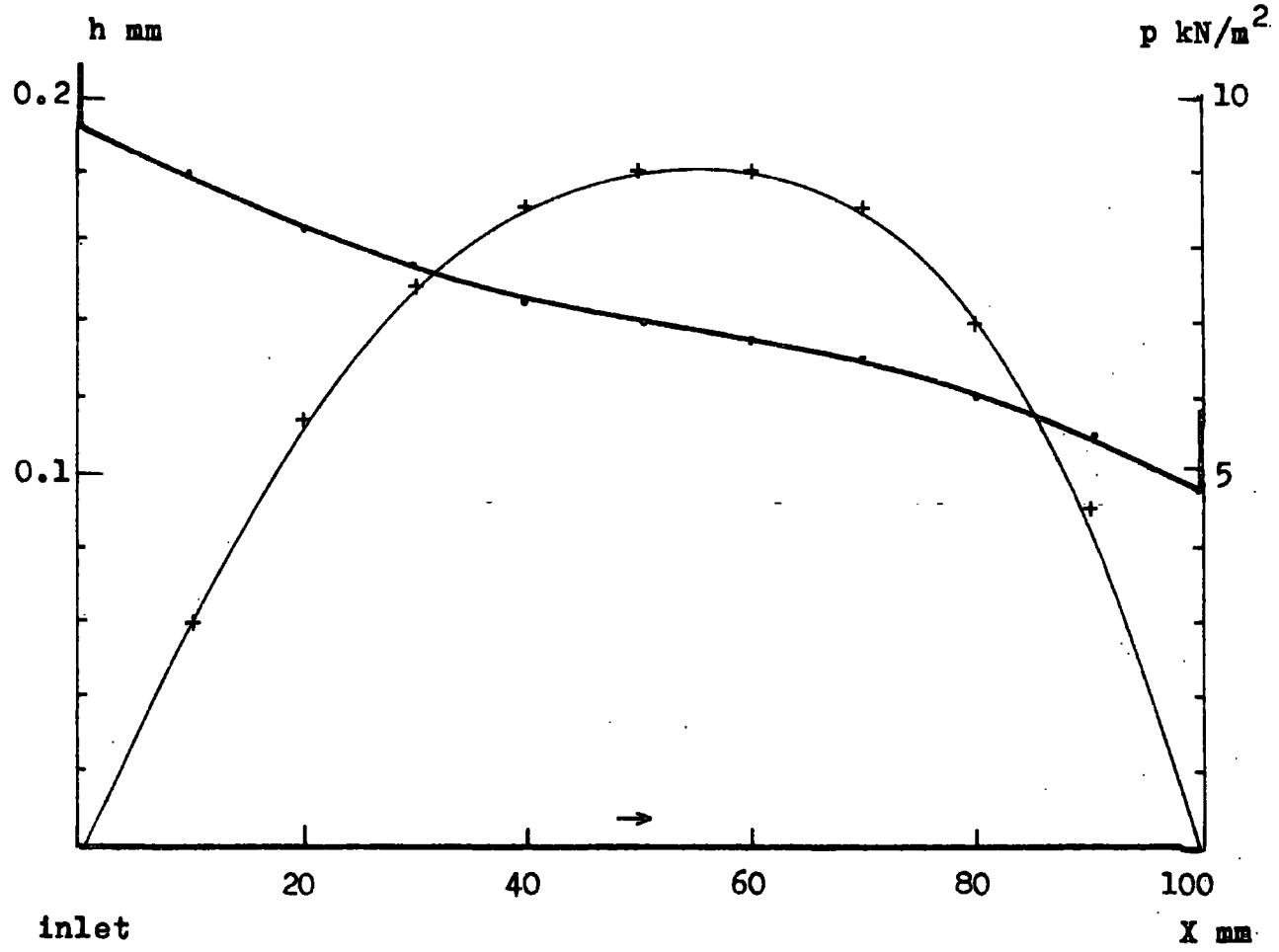

Variation in film thickness and pressure along the pad.

Graph 5.13b

p = 0.405
K = 0.86
W^x = 0.124
Ju = 0.545 N/m
Δ = 0.165 mm

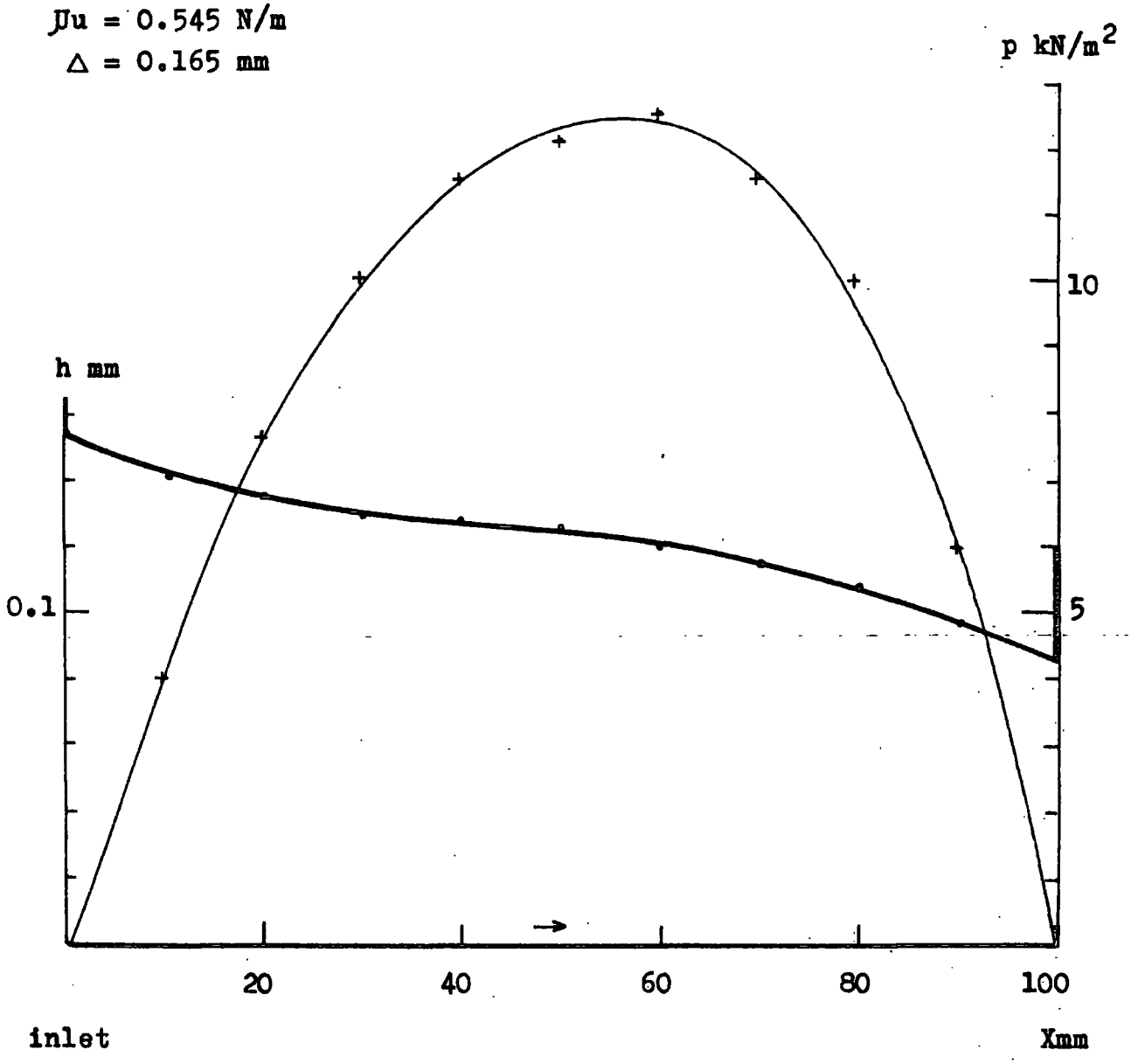

Variation in film thickness and pressure along the pad.

Graph 5,13c

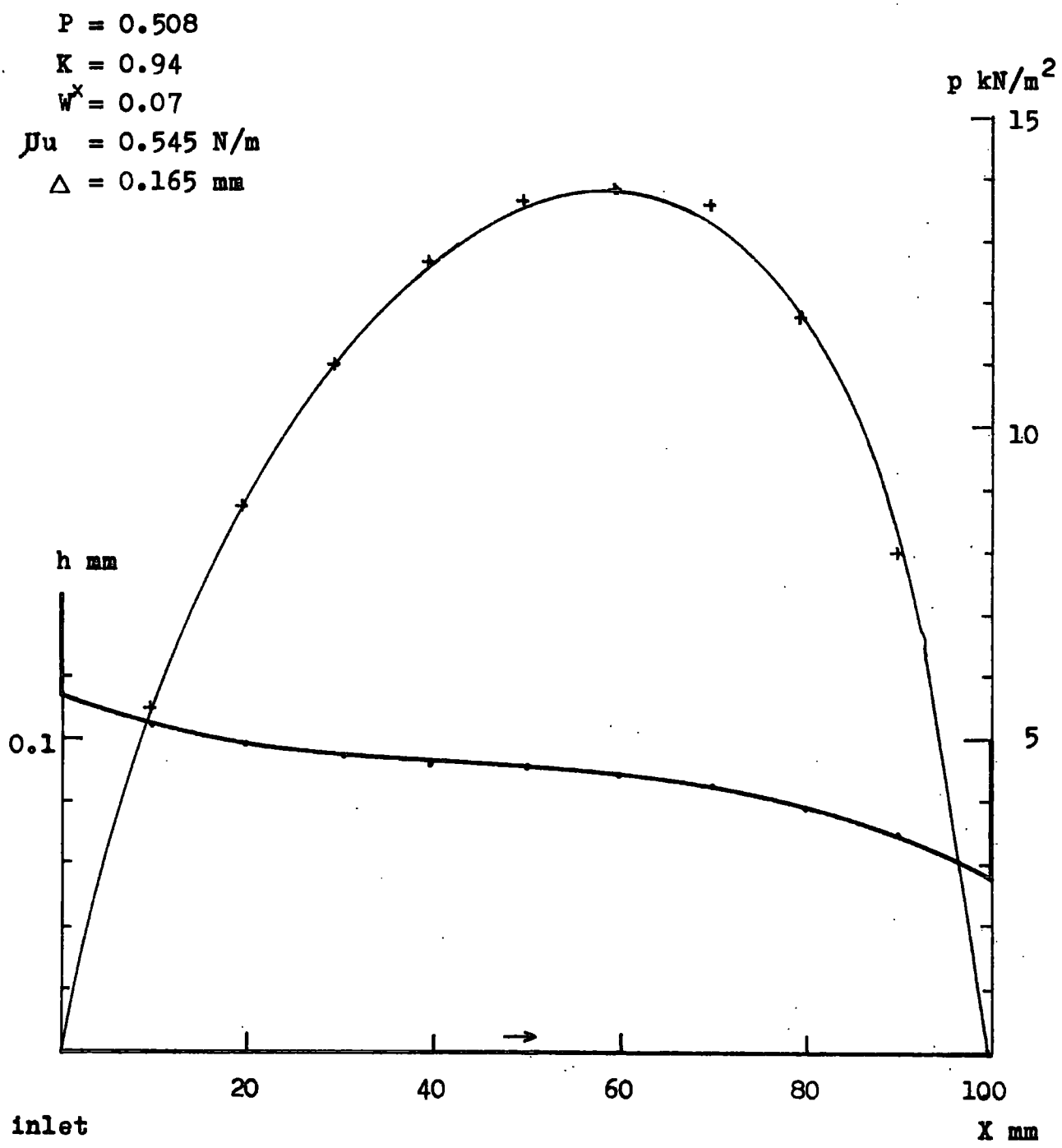

Variation in film thickness and pressure along the pad.

Graph 5.13d

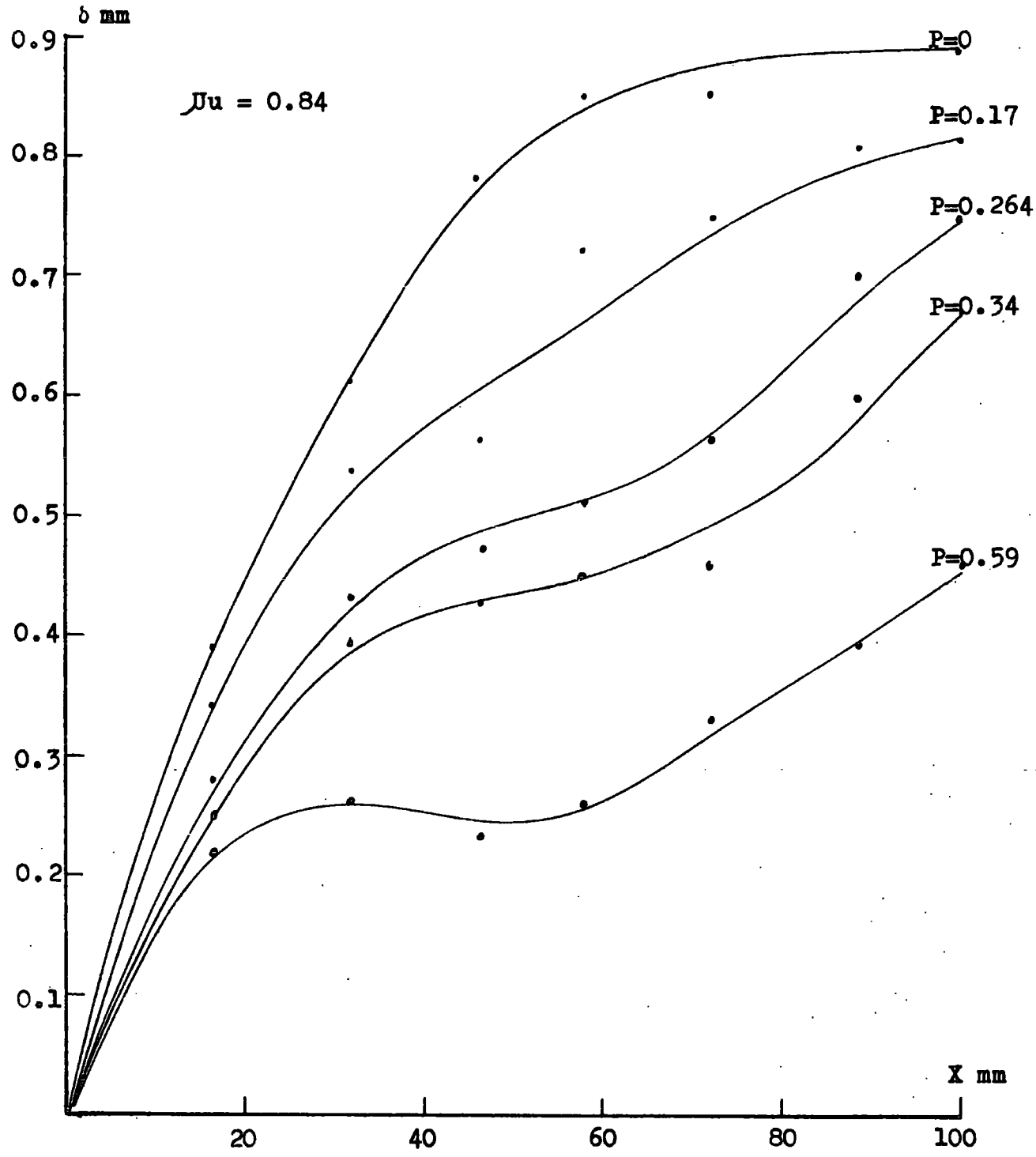

Pad profile.

Graph 5.14

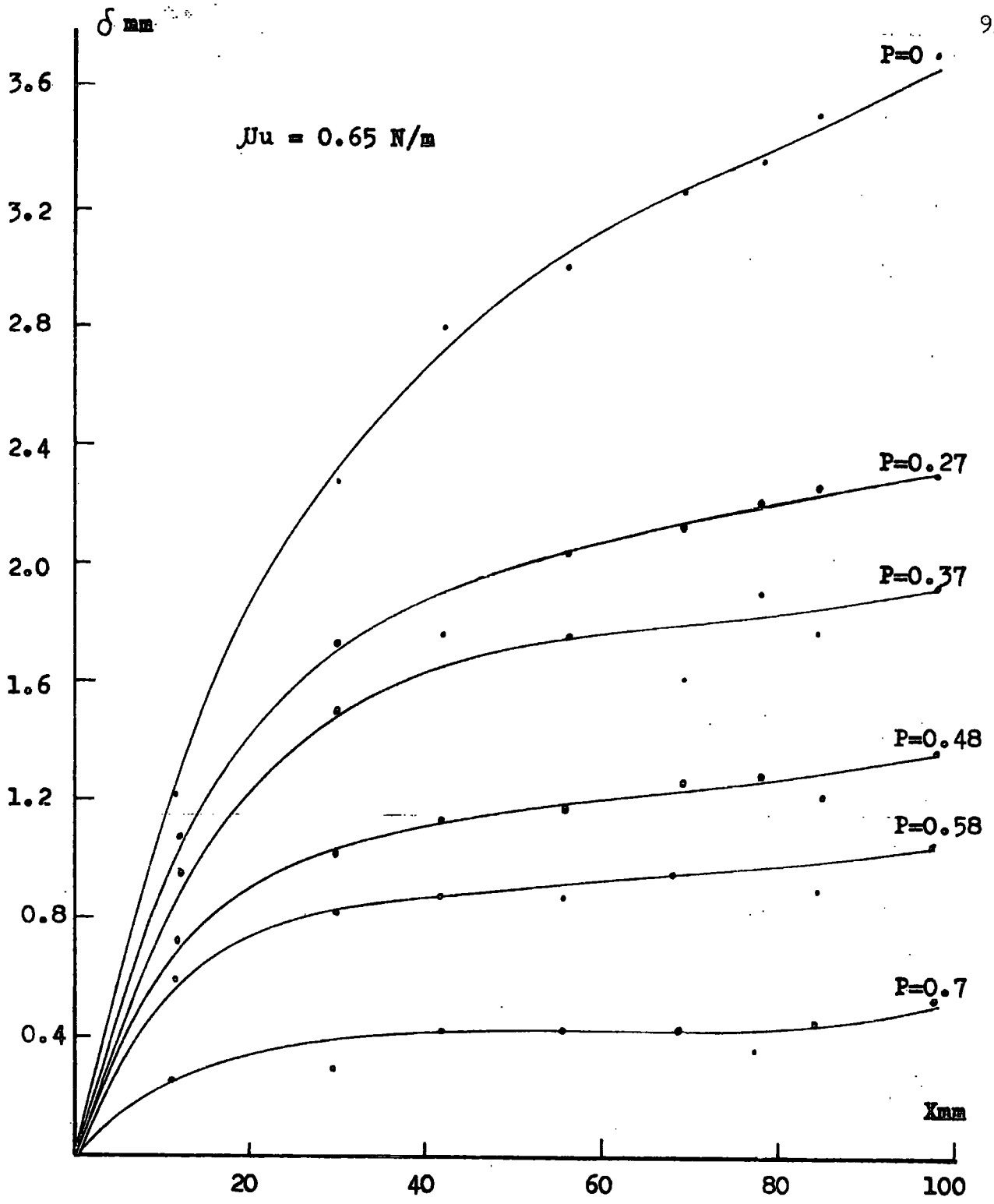

Pad profile.

Graph 5.15

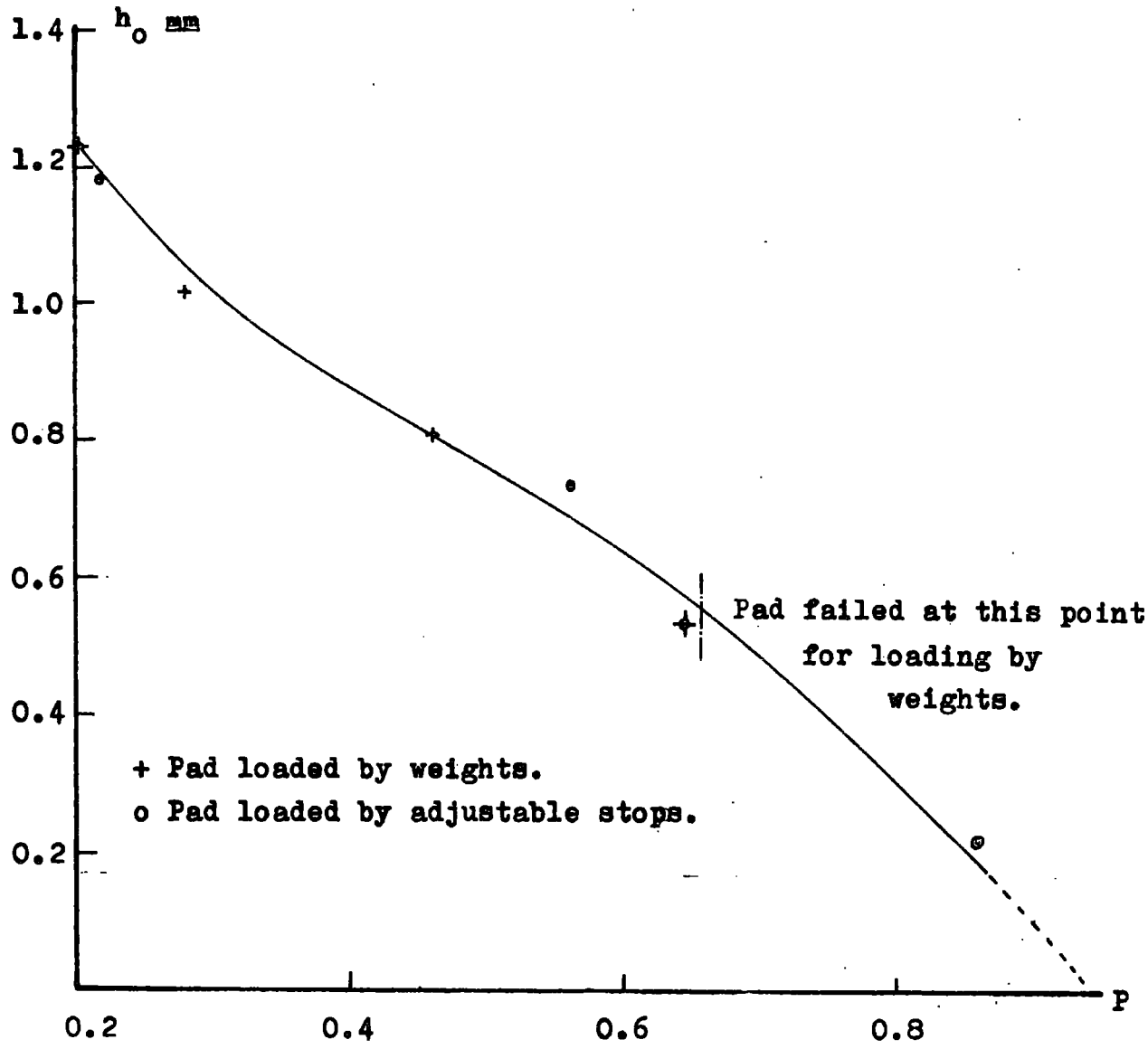

Variation in outlet film thickness with the pressure no. for the two types of loading process.

Graph 5.16

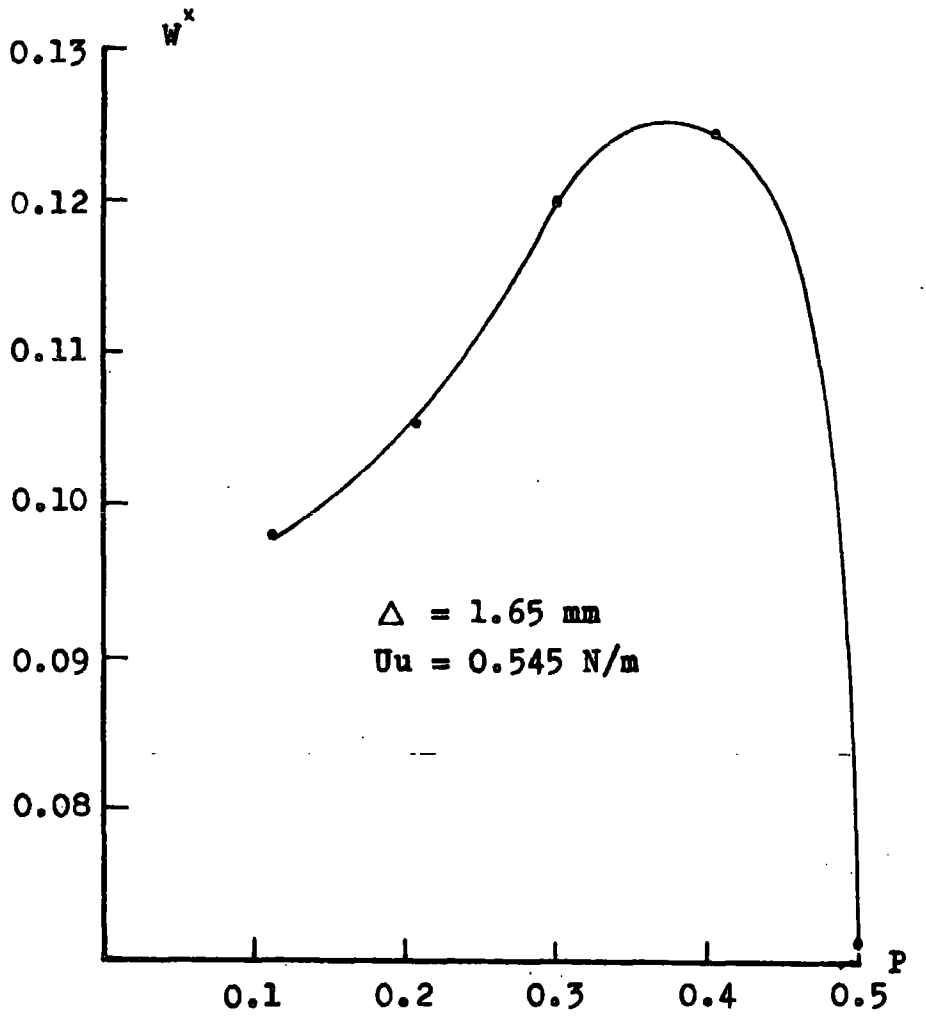

Load carrying capacity v Pressure no.
Film ratio constant.

Graph 5.17

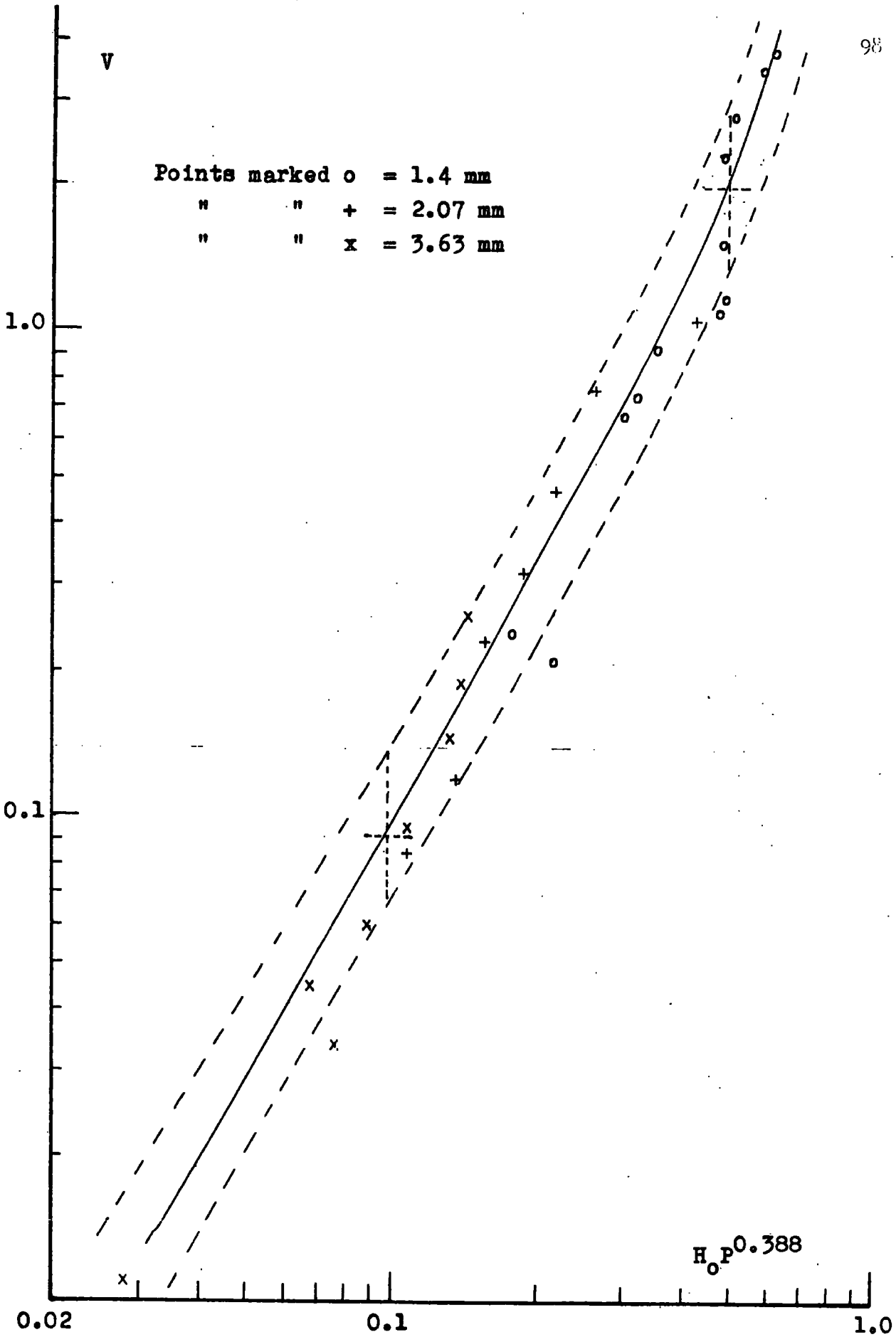

Comparison between experiment and the simple theory.

Plotted in the form $H_o P^{0.388}$ = Function(V)

Graph 5.19

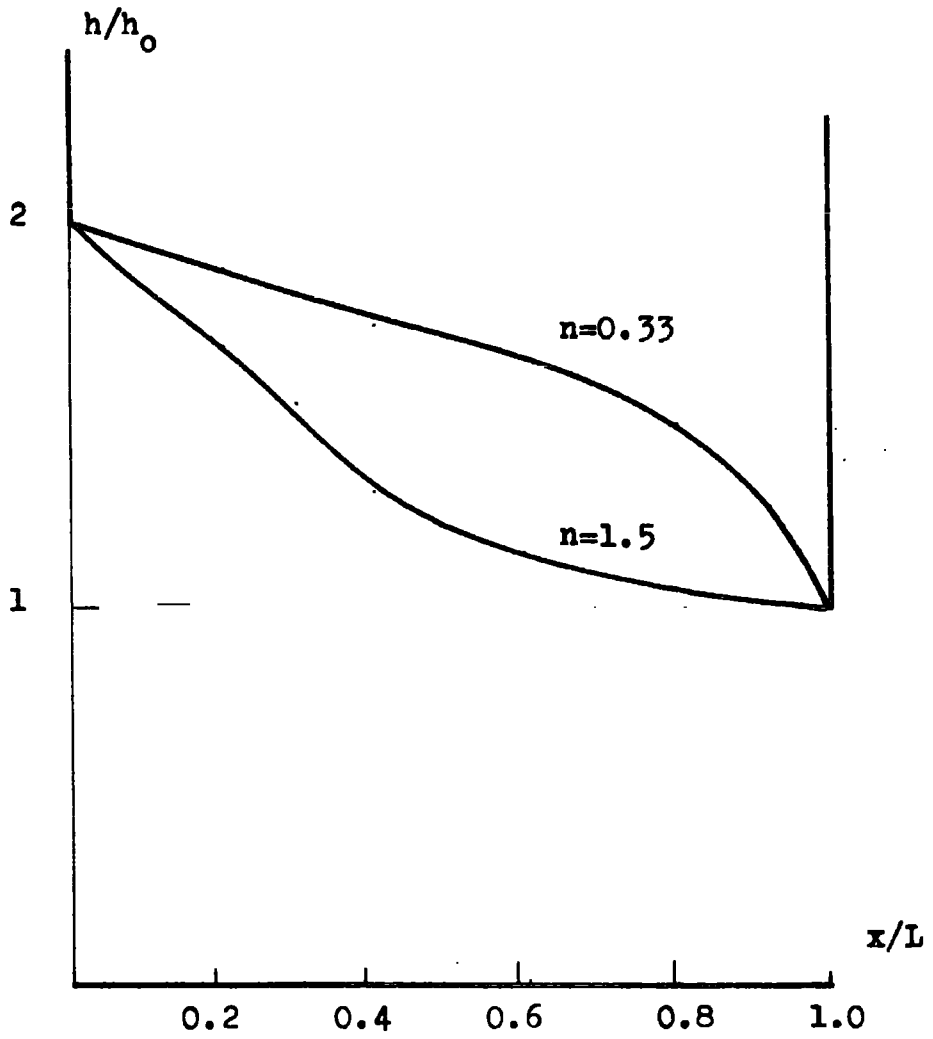

Surface profile generated by $h/h_o = \frac{2}{2 - \left[\frac{x}{L}\right]^n}$

Graph 6.0

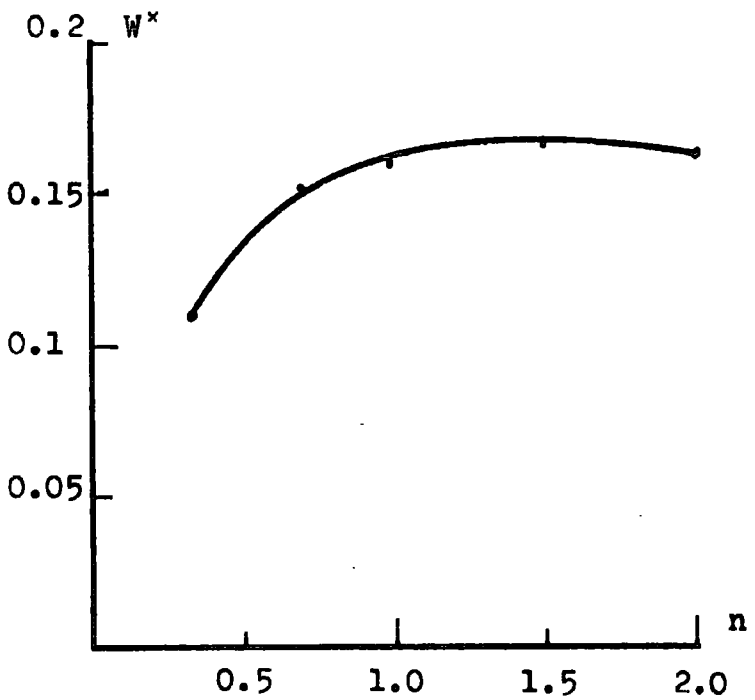

Effect of the surface profile on load capacity.

Graph 6.1

REFERENCES

1	Reynolds, O	"On the theory of lubrication and its application to Mr. Beauchamp Towers experiments". Phil. Trans. Roy. Soc. London Vol 177 1886
2	Beauchamp Tower	"1st Report on Friction Experiments" Proc. Inst. Mech. Eng. 1883
3	Neal, P.B.	"Film Lubrication of plane faced thrust pads" Proc. Lub and Wear Convention. 1963
4	Michell, A.G.M.	"Progress in Fluid Film Lubrication" Trans A.S.M.E. (1929) 51
5	Guerin and Hall	"Some Characteristics of Conventional Tilting Pad Thrust Bearings". Proc. Lub and Wear Convention. 1957
6	Hemingway, E.W.	"Experimental observations on ball mounted tilting thrust pads" Tribology Convention. 1968
7	Bennett A.H. and Ettles, C	"A self-acting parallel surface thrust bearing". Tribology Convention. 1968
8	Hemingway, E.W.	"A performance investigation into the elastically stepped and shrouded thrust bearing". Proc. I. Mech. E. 1967 Vol. 182 38
9	Pinkus and Sternlicht	"Theory of Hydrodynamic Lubrication" McGraw Hill
10	Goodier J.N.	"Stress distribution in rectangular blocks". Trans. A.S.M.E. Vol. 54 1932